To appear in *Transport Processes in Bubbles, Drops & Particles*, 2nd Ed.
Ed. R. Chhabra, D. De Kee, (Taylor & Francis, 2001).

Steady and Transient Motion of Spherical Particles in Viscoelastic Liquids

Gareth H. McKinley
Department of Mechanical Engineering
MIT, Cambridge, MA 02139, USA

1. Introduction

The motion of a spherical particle through a fluid with non-Newtonian rheological properties is a well-studied problem with a broad range of practical application from sedimentation of muds and slurries to processing of filled polymer melts. As a benchmark problem for computational rheology and the evaluation of numerical codes (cf. Hassager, 1988), the sedimentation of a sphere in an elastic fluid has become one of the most studied problems in non-Newtonian fluid mechanics. Almost 10 years ago, in the first edition of this book, Walters & Tanner (1992) provided a comprehensive overview of the state of knowledge at that time. Over the past decade, significant advances have been made in numerical algorithms for steady and transient computation of viscoelastic flows and also in quantitative experimental techniques for non-invasively resolving the spatial and temporal characteristics of both the particle motion and the velocity field within the fluid. These advances, when combined with careful rheological characterization of the test fluids studied and simulated, have led to a greater understanding of the motion of particles in complex fluids. This chapter focuses on these recent developments rather than comprehensively reviewing the early literature and should thus be regarded as complementary to the earlier reviews of Walters & Tanner (1992) and Chhabra (1993). We focus almost exclusively on motion in viscoelastic liquids, since these are the most common types of non-Newtonian fluids encountered and because the interactions of viscosity, elasticity and particle inertia give rise to some of the most complex and unexpected classes of phenomena. The motion of spheres through inelastic fluids such as power-law, Carreau or Bingham fluids is covered elsewhere in this book.

In order to avoid the additional complications arising from fluid inertia, most fundamental studies over the past decade have focused on the creeping motion of a sphere at low Reynolds numbers. In addition to its central role as a benchmark problem for rheologists and fluid dynamicists, such a problem continues to be of great practical relevance due to modern technological developments in, for example, highly-filled polymeric nanocomposites containing submicron spherical (or other shaped) particles and the use of submicron spherical beads as

'microrheometry probes' in diffusing wave spectroscopy (see for example Levine & Lubenksy 2001).

We begin by considering the motion of a single particle and the competing roles of different aspects of the flow geometry (e.g. wall effects) and fluid rheology (e.g. rate dependence of the material functions, and the finite extensibility of the molecules). We then proceed to consider the interactions of the inertial timescale of the particles and the relaxation timescale of the fluid on transient motions and then the interactions of multiple spheroidal particles.

2. Steady Sedimentation of a Single Sphere through a Viscoelastic Fluid

2.1 Problem Definition and Dimensional Analysis

The prototypical problem of interest is shown schematically in Figure 1. A rigid spherical object of radius a and density ρ_s settles under gravity in a container of characteristic size R. The viscoelastic fluid medium in the container is characterized by a density ρ, a zero-shear-rate viscosity η_0 and a characteristic relaxation time λ. The polymeric fluid may also contain a solvent of viscosity η_s and may also be shear thinning. The flow kinematics are a complex mixture of biaxial extension near the forward stagnation point, followed by strong shearing deformation near the bounding walls in the gap between the sphere and the wall and finally uniaxial extension in the wake. The relative importance of each term depends on the fluid rheology, the settling speed and also on the relative size of the sphere and the tube. The absence of geometric singularities such as sharp corners or stick-slip transitions would appear to make the problem amenable to numerical computation. Such expectations are often confounded by the kinematic complexity of the flow and the resulting boundary layers that develop in the stress field as we discuss further below.

In an experiment the terminal settling velocity of the particle at steady state is unknown *a priori* and must be measured experimentally using, for example photographic analysis (Jones et al. 1994), digital video-imaging (Becker et al. 1994), ultrasonic techniques (Watanabe et al. 1998) or magnetic resonance imaging. Dimensional analysis thus suggests that a convenient way of representing the problem is

$$\frac{\lambda U_s}{a} = f\left(\frac{a}{R}, \frac{\lambda\eta_0}{\rho a^2}, \frac{\rho_s}{\rho}, \frac{\eta_s}{\eta_0}, \frac{\eta(\dot{\gamma})}{\eta_0}\right) \tag{1}$$

where a/R is the radius ratio characterizing the geometry, $\left(\lambda\eta_0/\rho a^2\right) \equiv De/Re = El$ is the elasticity number, η_s/η_0 is the solvent viscosity ratio, and ρ_s/ρ is the density contrast. Since the only role of the particle density is to drive sedimentation under a gravitational body force, the latter ratio can be better expressed as a dimensionless weight $F_w\lambda/(a^2\eta_0) = a(\rho_s - \rho)g\lambda/\eta_0$. The final dimensionless ratio generically indicates that the results will be a function of the precise form of the rheological function(s) describing the rate-dependence of the fluid's viscometric properties. Here the characteristic deformation rate for the sedimentation flow past the sphere is $\dot{\gamma}_s = U_s/a$. The product $\lambda U_s/a$ is most correctly referred to as a Deborah number since it characterizes the dimensionless ratio of the fluid relaxation time and the residence time of a particle near the sphere. The term Weissenberg number (with $Wi = \lambda\dot{\gamma}_s$, Bird et al. 1987) is frequently used interchangeably; however, this is only appropriate when the boundaries are far from the sphere. For the case of a tightly fitting sphere the characteristic velocity in the annular gap between the sphere is $V_{nip} = U_s/\left(1-(a/R)^2\right)$and the deformation rate in the gap can thus be considerably higher than the estimate U_s/a (cf. Degand & Walters, 1995).

By contrast to experiments, in a typical viscoelastic flow calculation a steady Eulerian reference frame (moving with a velocity U_s downwards in Fig. 1) is selected such that the sphere remains stationary with velocity zero. The problem is non-dimensionalized with this velocity plus the sphere radius *a* and the fluid viscosity η_0. In this frame, the walls of the container are thus moved upwards at a dimensionless velocity of 1 and the resulting dimensionless drag force on the sphere is computed as a function of the Deborah number $De = \lambda U_s/a$. Quantitative comparisons between experiments and computations must thus be carried out with care (for further details see the discussions of Mena et al. 1987 and Arigo et al. 1995).

Very few calculations or experimental studies have considered all of these multidimensional effects and typically various terms are taken to appropriate limits of zero or infinity respectively.

2.2 The Drag Coefficient for Creeping Flow Past an Unbounded Sphere

Inertial effects in the fluid and the constraining effects of the bounding container walls become negligible in the limits $El \to \infty$ and $a/R \to 0$. For an ideal elastic fluid or 'Boger fluid' (Boger 1977/78) the viscometric properties are approximately independent of the deformation rate and changes in the drag on a settling sphere of density $\rho_s/\rho > 1$ can only arise from elastic effects in the fluid. For the creeping flow of a sphere through an unbounded viscoelastic fluid measurements of the dimensional force on the sphere are typically represented in terms of a

dimensionless drag correction factor $X(De)$ which is the ratio of the measured drag coefficient compared to the well-known result for the Stokes drag on a sphere settling at a velocity $U^{Stokes} = 2(\rho_s - \rho)a^2 g/9\eta_0$ (corresponding to $F_D{}^{Stokes} = 6\pi a\eta_0 U^{Stokes}$). When this result is expressed in dimensionless form one obtains

$$X(De) = \frac{C_D(De)}{C_D(De=0)} = \frac{C_D(De)}{\left(24/Re\right)} \tag{2}$$

where we have based the Reynolds number $Re = 2\rho a U^{Stokes}/\eta_0$ on the particle diameter to be consistent with the previous literature.

In figure 2 we show the measured dimensionless drag correction factor for a number of different ideal elastic fluids (Solomon & Muller 1996a). Figure 2(a) shows data replotted from oft-cited studies using a polyisobutylene-based (PIB/PB) Boger fluid (Tirtaatmadja et al. 1990) and a similar fluid formulated from polyacrylamide in corn syrup (PAA/CS) (Chhabra et al. 1980). At low Deborah numbers the drag ratio is unity before weakly decreasing in a manner consistent with perturbation theory for a second order fluid (Leslie & Tanner, 1961). As the density of the settling spheres is increased and the Deborah numbers exceed $De \geq 1$ the results diverge with markedly different behavior observed for the two apparently viscometrically-similar fluids. Additional measurements by Solomon & Muller for a series of elastic fluids formulated of monodisperse high molecular weight polystyrene dissolved in oligomeric styrene are shown in Figure 2(b). In each fluid the drag coefficient was observed to increase dramatically at high *De;* at the highest Deborah numbers the settling speed is decreased by a factor of three or more. Independent light-scattering and viscometric measurements were used to determine the thermodynamic quality of the solvent as noted in the caption and the authors noted a complex interplay between the solvent quality and the extensibility of the molecules. Similar extravagant drag enhancement effects have also been noted by Jones et al. (1994); however the latter data were obtained in a polyacrylamide-based fluid similar to that shown in Figure 2(a) exhibiting a monotonic decrease in the drag coefficient. In order to rationalize these complex trends in the evolution of the drag coefficient it is necessary to consider the rheological properties of the test fluids in greater detail.

2.2.1 The Role Of Fluid Rheology

At low Deborah numbers *De* << 1, nonlinear elastic effects such as normal stress differences (arising from shear or extension) are expected to be negligible in each of the elastic test fluids. The deformation history experienced by a fluid particle flowing past the sphere is essentially a Lagrangian unsteady shear flow. A reciprocal theorem can be used to compute the

first elastic correction to the total drag on the sphere from the known Stokes flow result valid at $De = 0$ without having to compute the full correction to the velocity field (Chilcott et al. 1988; Becker et al. 1994). However, since the first correction to the symmetric Stokes velocity field is anti-symmetric, the initial changes to the drag do not in fact occur until $O(De^2)$. For the Oldroyd-B fluid that is commonly used to characterize Boger fluids (Mackay & Boger 1988) the drag coefficient can be expressed as (Bird et al. 1987)

$$C_D = \frac{24}{Re}\left[1 - \frac{1}{2275}\left(\frac{401}{11} - \frac{39\eta_s}{\eta_0}\right)\left(1 - \frac{\eta_s}{\eta_0}\right)De^2\right] \tag{3}$$

At this point, it is helpful to recall that in a homogeneous shearing deformation started from rest the total shear stress for an ideal elastic polymer solution described by the Oldroyd-B model is given by

$$\tau_{yx} = \left[\eta_s + \eta_p\left(1 - \exp(-t/\lambda)\right)\right]\dot{\gamma}_{yx} \tag{4}$$

where $\eta_p \equiv \left(\eta_0 - \eta_s\right)$ is the polymeric contribution to the total viscosity. Since the deformation history of a material element flowing past the sphere is unsteady the viscoelastic contribution to the stress may not be given sufficient time to attain steady state. Indeed, as the Deborah number is slowly incremented the residence time of a fluid element ($t \sim a/U_s$) decreases and thus the elastic contribution to the total viscous drag on the sphere also decreases. The bulk of the drag is thus carried by the solvent and the drag correction factor may be expected to decrease below one by a maximum factor of η_s/η_0.

As the Deborah number exceeds values of $O(1)$ extensional effects in the wake begin to become important. The motion of a fluid element on the centerline of the tube in the wake of a sphere is characterized by an inhomogeneous extensional deformation. The long residence time of molecules passing close to the stagnation points can result in very large molecular elongations and thus very large elastic stresses. Solomon & Muller (1996b) also measured the transient extensional viscosity of the test fluids using a filament stretching rheometer. Such devices impose a uniaxial deformation history on a fluid element and measure the transient evolution in the extensional stress (see McKinley & Sridhar, 2002 for further details). All of the polystyrene fluids studied by Solomon & Muller showed very pronounced strain-hardening as expected, with dimensionless extensional viscosities (or Trouton ratios) of O(1000). This increase in the extensional viscosity with increasing molecular weight was found to correlate with the increase in the drag coefficient. However the authors also found a complex dependence of the elastic drag enhancement with the thermodynamic quality of the Newtonian solvent. This competing

interplay between molecular weight (M_w) and solvent quality (as characterized by the scaling exponent ν ; Doi, 1997) can be understood by noting that for a dilute polymer solution, Zimm theory predicts that the characteristic fluid relaxation time scales as $\lambda \sim M_w^{3\nu-1}$ whereas the dimensionless extensibility of the molecules (which sets the magnitude of the extensional viscosity) varies as $L \equiv R_{\max}/R_g \sim M_w^{1-\nu}$.

In polyelectrolytes such as polyacrylamide (PAA) the degree of hydrolysis and the total ionic strength are also important in controlling the viscometric properties. The presence of salt can screen intra-chain repulsions and reduce the equilibrium coil size of the chain and the longest relaxation time whilst increasing the extensibility of the molecules. Solomon & Muller (1996a) note that this additional complexity may partially explain the differences between the observations of Chhabra et al. (1980) and Jones et al. (1994) using nominally-similar PAA/CS elastic fluids. In addition it is now recognized that even small amounts of shear-thinning in the polymeric contribution to the viscosity $\eta_p(\dot{\gamma})$ (which are usually obscured on a logarithmic scale) can be significant when considering a 25% reduction in the drag coefficient as depicted in Figure 2.

2.2.2 Stress-Conformation Hysteresis

In contrast to the experimental measurements shown above, numerical simulations for the drag on a sphere in an unbounded viscoelastic fluid show remarkably little change in the drag coefficient. Gervang et al. (1992) computed the flow field using a spectral method and the Oldroyd-B model with several values of the solvent viscosity ratio η_s/η_0. They found good agreement with eq. (3) at very low *De* with an 0.2% drag decrease at $De \approx 0.5$. followed by a moderate drag enhancement of less than 3% before loss of convergence at $De \approx 2.0$. Chilcott & Rallison (1988) considered numerical simulations of a finitely-extensible dumbbell model (FENE-CR model) and showed that the extent of the drag increase depends on the finite extensibility of the molecules; however drag increases could only be obtained for moderate values of the extensibility parameter ($L^2 \sim 10$) that are not consistent with molecular estimates for a dilute solution (typically $L^2 \geq 1000$). Although this discrepancy between experiments and computations has not been definitively resolved, significant insight over the past 5 years has been made by recognizing that the process of molecular unraveling in a strong extensional flow is much more complex than is described by the inverse Langevin or FENE force laws which are derived from *equilibrium* statistical mechanics. Brownian dynamics simulations (van den Brule, 1993; Rallison, 1997; Doyle et al. 1998; Larson et al. 1999) reveal a wide range of

intramolecular configurations; many of which can be directly observed in fluorescence imaging microscopy of DNA solutions (Smith & Chu, 1998). Since these configurations are not the most probable ones expected from equilibrium statistics they are associated with lower entropies and higher internal tensions. The rapid relaxation of these configurations following the cessation of stretching (or a lowering of the stretch rate below a critical coil-stretch value of $De \approx 0.5$) make the resulting stresses appear 'viscous-like'; however, careful analysis shows they are in fact elastic in origin (Doyle & Shaqfeh, 1998). On a macroscopic basis the non-equilibrium nature of the internal molecular configurations results in a stress-conformation hysteresis which can be measured by simultaneous measurements of the total polymeric stress and the molecular configuration using independent mechanical and optical techniques (Doyle et al. 1997; Sridhar et al. 2000). The resulting hysteresis loops result in the additional dissipation of mechanical work rather than the entropic storage and return of energy.

The unsuitability of the equilibrium entropic spring for describing fast transient extensional flows was first discussed by Ryskin (1988) when modeling the enhanced pressure drop observed in converging flow of dilute polymer solutions. More recent studies (Sizaire et al. 1999; Ghosh et al. 2001) have shown that the hysteresis arises from both internal configurational changes in the conformations of individual molecules and from non-Gaussian behavior of the ensemble distribution of molecules. Recent work by Li & Larson (2001) shows that the extent of the hysteresis is very sensitive to small changes in the solvent quality parameter ν and the magnitude of the hysteresis increases as the thermodynamic quality of the solvent increases. Since the area enclosed by the hysteresis loop should provide a measure of the external flow work that is dissipated viscously rather than elastically stored and returned this should correspond to a higher elastic drag correction factor. This enhanced stress-conformation hysteresis is consistent with the experiments of Solomon & Muller shown in Figure 2(b).

It is worth noting that almost all Brownian dynamics studies to date have considered homogeneous shearing and/or extensional flows rather than the nonhomogeneous kinematics characteristic of flow past a sedimenting sphere. Experimental measurements of the local velocity field and the stress-conformation hysteresis combined with Brownian dynamics calculations of the internal structure of a bead-spring chain may help yield additional insight into the response of long chain molecules in a complex flow and the resulting modifications to macroscopic quantities such as the drag coefficient.

2.3 Wall Effects

2.3.1 The Wall Correction Factor

The drag correction factor $X(De)$ defined in eq. (2) is determined experimentally by performing experiments in large containers of viscoelastic fluid. Care must be taken to ensure that the effects of the bounding walls are carefully accounted for, since the effects of rigid boundaries play an extremely important role in creeping flows of viscous fluids. In a viscous Newtonian fluid, velocity perturbations from a sedimenting sphere will extend to the Oseen length $\ell \sim a/Re$ which may be greater than the bounding wall of radius *R*. The drag is thus modified from that expected in an unbounded fluid. At steady state the drag force resulting from the fluid motion between the spheres and the no-slip boundary balances the weight of the particle. By convention the effects of the walls and of fluid elasticity are expressed in terms of a drag correction factor $K(a/R, De)$ which measures the relative change in the drag force of the sphere compared to the equivalent Stokes' drag for creeping flow

$$6\pi a \eta_0 U_s K = F_w \equiv \tfrac{4}{3}\pi a^3 \left(\rho_s - \rho\right) g \tag{5}$$

Or, equivalently, by substituting for the Stokes settling velocity in an unbounded Newtonian fluid:

$$K(a/R, De) = \frac{U^{Stokes}}{U_s} \tag{6}$$

The correction factor thus incorporates the effects of both elasticity and the geometric radius ratio. In experiments, spheres of known size and density contrast are dropped in a sequence of successively larger tanks of viscoelastic fluid and the results are extrapolated to $a/R \to 0$. Care must be exercised with this extrapolation since it does not occur at constant *De*; the experiments are typically performed at fixed dimensionless weight and changing the radius ratio thus indirectly also affects the Deborah number $De = \lambda(U_s/K)/a$!

Extensive efforts have been made to experimentally and numerically determine this drag correction factor for a variety of viscoelastic fluids. The generic form of the resulting data for the creeping motion of an ideal elastic fluid (i.e. with $E \to \infty$, $\eta(\dot{\gamma})/\eta_0 = 1$ and η_s/η_0 fixed in equation 1) is shown schematically in Figure 3(a) as a two-dimensional surface. Specific measurements for a semi-dilute PIB/PB Boger fluid corresponding to two sections through this surface are also shown in Figure 3(b). For Newtonian fluids (*De* = 0) the drag correction factor reduces to the well-known Faxén correction (Happel & Brenner, 1964) which is commonly expressed in the form

$$K_N(a/R) \equiv \frac{1}{1 - f(a/R)} \tag{7}$$

with

$$\begin{aligned} f(a/R) = \big[& 2.10444(a/R) - 2.08877(a/R)^3 + 0.94813(a/R)^5 \\ & + 1.372(a/R)^6 - 3.87(a/R)^8 + 4.19(a/R)^{10} ... \big] \end{aligned} \tag{8}$$

For $a/R = 0.243$ one obtains K_N = 1.932 and for $a/R = 0.121$, K_N = 1.335. As in the unbounded case the first effects of elasticity appear to generally be to reduce the drag correction below the Newtonian value due to the rheological unsteadiness of the shearing flow around the sphere. However, in contrast to the first elastic corrections to the unbounded drag correction factor $C_D(De)$, these effects typically appear at first order in the radius ratio (see for example the early work of Chhabra et al, 1981; 1988) and thus a linear extrapolation to $a/R \to 0$ to determine $X(De)$ can be safely employed for experiments at low *De*. For moderate *De*, wall effects appear to be less important than in the motion of the corresponding Newtonian fluid. At higher *De* the drag increases again and the magnitude of the drag enhancement is clearly a strong function of both the radius ratio and the fluid elasticity. Similar trends are also observed in the closely related experimental configuration of cross-flow of a viscoelastic fluid past a cylinder constrained on the centerline of a planar channel (Huang & Feng, 1995; Liu, 1997).

2.3.2 Numerical Computation of Wall Effects in Elastic Fluids

Extensive studies of the interaction of the flow kinematics and the rheological properties of the constitutive model can be found in the studies of Lunsmann et al. (1993); Satrape & Crochet (1994); Arigo et al. (1995), Rasmussen & Hassager (1996) and Yang & Khomami (1999). Although multi-mode finitely-extensible dumbbell models are able to qualitatively capture the initial decrease and subsequent increase in the drag correction factor, none of these dumbbell based models is capable of describing the experimental data quantitatively over a wide range of *De* and in different tube to sphere radius ratios. The reason for this failure is most likely due to the incorrect modeling of the rapid transient molecular extension in the fluid and the resulting stress-conformation hysteresis that is expected. Recent 'configuration field' computations with the molecularly-based FENE dumbbell model (i.e. without the Peterlin closure required to obtain a closed form constitutive equation) show that the distributional hysteresis incorporated by the model does slightly increase the drag above that of the closed form model but only by a few percent (Yang & Khomami, 1999). Similar calculations are

needed using bead-spring chain models with internal configurational degrees of freedom capable of resolving the complex kinked & looped structures observed in transient extensional flow experiments (Smith & Chu, 1998; Li et al. 2000)

The computation of the drag correction factor for the creeping flow of an Upper-Convected Maxwell fluid ($\eta_s/\eta_0 = 0$) past a sphere in a tube with $a/R = 0.5$ was selected as an international numerical benchmark problem in 1988. The problem remains a challenge to this day due to the stress boundary layers that develop near the rigid walls of the sphere and the tube. The current status for this benchmark problem has been reviewed by Warichet & Legat (1997) and Baaijens (1998). The most recent data are summarized in Figure 4. The drag correction factor decreases from K_N = 5.947 and reaches a plateau value of $K \approx 4.04$ at $De \approx 2$. For larger Deborah numbers the agreement between different numerical methods becomes less satisfactory, however it appears that the drag begins to slowly increase again before convergence is lost. In general for large radius ratios ($a/R \geq 0.25$) computations show that the largest stresses are found not in the extensional wake but in the nip between the sphere and the wall and in retrospect the ratio $a/R = 0.5$ may not have been optimal. At subsequent numerical workshops the ratios $a/R = 0.125, 0.25$ have been proposed as additional benchmark problems (Brown & McKinley 1994).

These benchmark problems have proven useful in demonstrating that mesh-converged and internationally-consistent results can be obtained with a number of different numerical methods given sufficient care; however extending the domain of convergence to progressively higher *De* has proven difficult. Even though the flow lacks geometric singularities, sharp gradients (particularly in the polymeric stresses) develop near the rigid boundary which require special high-order techniques to accurately resolve (see for example Yuran & Crochet, 1995; Owens & Phillips 1996; Fan et al. 1999; Chauvière & Owens, 2000). Similar convergence difficulties plague the analogous problem of flow past a cylinder in a channel (see Alves et al. (2001) for a summary of recent progress in this geometry). A boundary layer analysis for both the extensional stress in the wake (Harlen 1990) and the polymeric stresses near the curved rigid surface of the object (Renardy, 2000) may be more appropriate for studies at very high *De* but at present problems remain to be resolved with respect to the appropriate inlet conditions – which are determined in practice by the upstream flow near the nose of the object. Ultimately a hybrid technique in which a potential-flow–like 'outer region' is patched to an inner viscometric-like boundary-layer domain may prove to be the optimal way forward.

Time-dependent two- and three-dimensional calculations (Brown et al. 1993; Smith et al. 2000) and linear stability analysis of the local stagnation flow (Öztekin et al. 1997) also suggest

that both the sphere/tube and cylinder/channel problems may lose stability at high *De*. The transition from a steady two-dimensional motion to a three-dimensional steady flow consisting of periodic streamwise vortices in the wake of a cylinder has been observed experimentally using a constant-viscosity PIB/PB Boger fluid (McKinley et al. 1993). Early work by Bisgaard (1983) suggested the possibility of a wake instability behind a sphere settling in a shear-thinning polyethylene oxide (PEO/W) solution. However a number of subsequent LDV and DPIV studies of wake flows in elastic liquids have failed to duplicate these observations (see §2.3 for further details).

2.3.3 The Effects of Shear-Thinning on the Wall Correction Factor

Since the skin drag and the form drag both play large roles in determining the total drag on the sphere (Lunsmann et al. 1993) the deformation rate dependence of the material properties play a key role in determining the total drag correction factor.

Experimental results and correlations for weakly elastic fluids are reviewed in detail elsewhere by Chhabra (1993), and here we briefly mention recent developments of relevance to the present discussion. Perturbation results and empirical correlations for the drag coefficient in unbounded flows of purely inelastic fluid models such as the Carreau model have recently been discussed in detail by Rodrigue et al. (1996). A perturbation analysis for small shear rates shows that the drag coefficient varies in the same way as eq. (3)

$$C_D = \frac{24}{Re}\left[1 - \frac{6007}{10010}(1-n)(\Lambda\dot{\gamma}_s)^2 + O(\Lambda\dot{\gamma}_s)^4 \ldots\right] \tag{9}$$

where $\Lambda\dot{\gamma}_s << 1$ is the Carreau number characterizing the importance of shear-thinning. Energy dissipation arguments have also been used to evaluate the drag coefficient for power law fluids over a wide range of conditions (Ceylan et al. 1999). A detailed numerical and experimental study of wall effects in power-law fluids has recently been presented by Missirlis et al. (2001). By analogy to figure 3(a) the results can be expressed as a two dimensional surface $K(a/R, n)$ where *n* is the power law index. Interestingly the drag evolves in a non-monotonic way with *n* for $a/R \leq 0.125$ due to the interplay between wall effects and shear-thinning. In the limit $n \to 0$ the drag correction factor approaches a value that is independent of the presence of the bounding walls. This is due to the highly localized shear-thinning regions that form near the sphere surface. The resulting value of the drag correction factor would appear to be amenable to a boundary layer calculation but this has not yet been attempted.

Frequently, the dramatic shear-rate-dependent decreases in the viscosity that are characteristic of viscoelastic fluids such as polymer melts and polymer solutions overwhelm the moderate effects of fluid elasticity. In such cases, Mena et al. (1987) show that a simple rescaling of the Faxén correction factor to reflect the reduction in wall effects resulting from the lower viscosity at a characteristic deformation rate $\dot{\gamma}_s = U_s/a$ can capture the evolution in the drag. Eq (7) then becomes

$$\frac{U^{Stokes}}{U_s} \equiv K(a/R, \eta(\dot{\gamma}_s)/\eta_0) = \frac{\eta(\dot{\gamma}_s)/\eta_0}{1 - \dfrac{\eta(\dot{\gamma}_s)}{\eta_0} f(a/R)} \tag{10}$$

Mena et al. used a power model for the shear-rate dependence of the viscosity and eq. (10) thus diverges as $\dot{\gamma}_s \to 0$. Arigo & McKinley (1997) used a Carreau model and a multimode Phan-Thien–Tanner (PTT) model to fit the shear-thinning measured in a highly elastic concentrated solution of 2 wt% PAA in Glycerin and water (PAA/G/W). These models predict a bounded viscosity as $\dot{\gamma}_s \to 0$ and thus eq. (10) was found to provide a good description of the measured drag data for all of spheres examined (Arigo & McKinley, 1997).

2.3.4 Tightly Fitting Walls & More Complex Geometries

Tanner & Walters (1992) speculated on what would happen for spheres in tightly-fitting tubes such that $a/R \to 1$. The situation was subsequently investigated experimentally by Oh & Lee (1992) for the ratio a/R = 0.50, 0.66, 0.75, by Arigo et al. (1995) using a/R = 0.40, 0.63 and by Degand & Walters (1995) for a/R = 0.88. The latter experiments were also simulated numerically by Mitsoulis (1998) using a number of viscoelastic constitutive models. Interestingly the drag correction $K(a/R, De)/K_N(a/R)$ for sedimenting spheres is found to *decrease* monotonically with increasing *De*. This is partially due to the shear-thinning in the rheological properties of some of the test fluids but is also a consequence of the general form of Figure 3(a). The rapid increase in the magnitude of the wall-correction factor overwhelms other effects and results in a very slow sedimentation velocity and thus very low Deborah numbers. At low *De* the drag correction is dominated by the initial Lagrangian unsteadiness of the flow. As we have noted in §2.2.1 the terminal velocity of a sedimenting sphere in a tube is given by eq. (6). Furthermore at low to moderate *De*, we expect the wall correction factor to drop to a minimum value $K_{\min} \approx (\eta_s/\eta_0) K_N(a/R)$. The maximum attainable Deborah number is thus expected to be in the range

$$De_{\max} = \frac{\lambda U_{s,\max}}{a} \approx \left(\frac{\lambda 2a(\rho_s - \rho)g}{9\eta_s} \right) \frac{1}{K_N(a/R)} \tag{11}$$

where $K_N(a/R)$ is the Faxén correction given by eq. (7). The divergence in K_N for large (a/R) can only be overcome by dropping extremely dense spheres of very large radius into high molecular weight solutions or perhaps by using centrifugation. This maximum Deborah number is not a function of the solvent viscosity since, for a dilute solution, Rouse-Zimm theory shows that the longest relaxation time in a fluid scales as $\lambda \sim [\eta]\eta_s M_w/(N_A k_B T)$. Here $[\eta]$ is the intrinsic viscosity which is a function of the solvent quality ($[\eta] \sim {M_w}^{3\nu-1}$) and is described by the Mark-Houwink equation (Brandrup et al. 1997). Degand & Walters were able to overcome this limitation by fixing the sphere in the tube and using a pressure-driven flow to attain high *De*. Although the far field boundary conditions are different for this configuration measurements of the pressure drop across the annular contraction between the sphere and the wall showed a strong increase at high *De* in agreement with the general form expected from Figure 3(a).

Most quantitative studies to date have focused on cylindrical geometries with the sphere sedimenting along the centerline. Joseph et al. (1994) have considered the sedimentation of more complex-shaped objects and their tendency to align in the flow direction. We return to these effects in §4. Ilic et al. (1992) have computed wall effects for settling of spheres through Newtonian fluids in more complex shaped containers. Walters & Tanner (1992) discuss the phenomena of elastic-induced migration towards the wall and the sensitivity of experiments to initial imperfections in the alignment. In general it is found to very difficult to ensure that the sphere remains on the centerline for large radius ratios and the results discussed above should be considered valid for $a/R < 0.5$.

2.4 Elastic Effects on the Structure of the Wake

In addition to numerical computations and experimental observations of global measures such as the drag correction, a hallmark of studies over the past decade has been a detailed focus on the local structure of the fluid velocity field in the vicinity of the sphere. This has been driven in part because of the recognition that an integrated parameter such as the total drag is not a very sensitive measure of elastic modifications to the stress and velocity fields (see, for example, Chilcott & Rallison, 1988; Harlen 1990), and in part by experimental evidence of a flow instability in the wake (Bisgaard, 1983). These changes may be confined to very narrow regions in the wake where the fluid elements have experienced large transient extensional deformations. Early theoretical investigations and experimental studies focused on the question of whether

elasticity shifted the streamlines close to the sphere downstream or upstream with respect to the fore-aft symmetric Stokes flow. These results were frequently contradictory due to the range of rheological properties in the fluids studied and the possibilities of inertial effects and changes of type in the governing equation (cf. Delvaux & Crochet, 1990). These early studies are reviewed elsewhere (McKinley, 1991; Chhabra, 1993) and here we focus specifically on the extensional flow in the wake downstream of the rear stagnation flow. For clarity we distinguish between observations in ideal elastic dilute polymer solutions (i.e. 'Boger fluids') and those in shear-thinning viscoelastic liquids such as concentrated polymer solutions.

2.4.1 Constant Viscosity Elastic Fluids

By studying the wake structure in the creeping flow of ideal elastic fluids one can isolate the effects of the extensional flow from changes in the local fluid viscosity resulting from shear thinning. In figure 5 we show laser Doppler velocimetry (LDV) measurements of the axial component of the centerline velocity field upstream and downstream of spheres of increasing density (or dimensionless weight) in tube of fixed ratio a/R = 0.243 containing a PIB/PB Boger fluid ($El \approx 77$; $\eta_s/\eta_0 = 0.59$). As the density is increased the sedimentation velocity and the resulting Deborah number increase accordingly. When the results are non-dimensionalized and plots of $v_z(r=0, z/a)/U_s$ are examined, it becomes clear that although there is almost no viscoelastic modification to the velocity in the biaxial flow upstream of the sphere, the length of the downstream wake region is increased dramatically. Experiments for different sphere and tube sizes show that the axial extent of this elastic wake also depends on the radius ratio *a/R* and decreases as the magnitude of the wall effects increases (Arigo et al. 1995).

The fluid entering the biaxial flow is in an initially relaxed state and the small polymeric stresses that develop do not significantly modify the velocity field from the corresponding Newtonian stagnation profile. By contrast, as the molecules enter the extensional flow in the downstream wake they have been 'preconditioned' by the shearing flow near the sphere surface and partially oriented. The high molecular extension and resulting tensile stresses that then develop in the wake retard the subsequent decay in the velocity field. Similar observations of a downstream shift in the elastic wake behind a cylinder channel are also observed (McKinley et al. 1993). Birefringence measurements in the latter two-dimensional geometry are also possible and confirm the presence of very high molecular orientations in the wake (Baaijens et al. 1995).

Correlative techniques such as digital particle image velocimetry (DPIV) enable the quantitative measurement of the complete two-dimensional velocity field in viscoelastic flows

(Pakdel & McKinley, 1997). The dramatic extent of the elastic downstream wake can be seen in the velocity contours shown in Figure 6 (Fabris et al. 1999). The velocity in the wake decays slowly from a dimensionless value of 1 towards zero over a distance of 30 radii. Corresponding measurements of the drag showed that this wake development evolves in conjunction with the dramatic increase in $X(De)$ shown in Figure 2(b). The three dimensional structure of the wake behind a sphere in a rectangular container have also been studied by Harrison et al. (2001)

This downstream shift in the wake structure behind the sphere has often been qualitatively described as similar to the inertial shift seen in moderate Reynolds number flows of Newtonian fluids. However, the elastic wake shift scales with the Deborah number and occurs even in creeping flows (corresponding to $E = De/Re \to \infty$). In addition this slow decay of the fluid velocity has been found to be monotonic and stable in all experimental studies to date.

Numerical calculations of an enhanced elastic drag must thus also capture this extended elastic wake structure. Simulations with FENE dumbbell models are able to qualitatively describe the downstream shift but the effect is much smaller than is observed experimentally. The results of finite element simulations using the FENE-CR and multimode Phan-Thien–Tanner (PTT) model are also shown for comparison in figure 5 at Deborah numbers corresponding to the experimental measurements. Similar curves are obtained for a wide range of constitutive models (Bush, 1993; Lunsmann et al. 1993; Yang & Khomami 1999) It is becoming increasingly clear that the discrepancy between the extravagant shifts in the wake observed experimentally and the more modest changes predicted computationally is connected with the stress-conformation hysteresis expected in fast transient extensional flows (see §2.1.2). In a conventional FENE model the work stored in the entropic-elastic spring is returned without loss and this can drive a 'recoil-like' flow in the wake which assists in driving the recovery of the velocity field. This elastic energy storage and return also explains why the elastic drag coefficient computed for large finite extensibility parameters $L^2 \sim O(1000)$ monotonically decreases below the corresponding Newtonian value. In order to obtain drag enhancements it is presently necessary to use unphysically low values of L so that the FENE dumbbells approach their maximum extension (see for example Chilcott & Rallison, 1988; Yang & Khomami 1999). In this limit the dumbbells act as inextensible rods and viscously dissipate energy. This rod-like dissipation leads to the increase in the drag force on the sphere.

Experiments and computations with more realistic bead-rod and bead-spring chain models suggest that local regions of real molecules become almost fully extended far more rapidly than predicted by affine deformation of a dumbbell or fluid element and thus dissipate more of the external flow work due to coil-stretch hysteresis (as envisioned by the 'yo-yo'

picture of Ryskin, 1987). Recent Brownian dynamics calculations with bead-spring chains in a model inhomogeneous extensional flow do indeed show such a hysteresis (Hernández Cifre & de la Torre, 1998). The large computational requirements presently preclude the complete simulation of complex flows with such bead-rod or bead-spring chains. A possible way to describe the stress-conformation hysteresis may thus be to develop kinetic theory-based models in which the effective dumbbell extensibility $L(t)$ evolves in time depending on the flow history experienced by the molecules in order to mimic the different distribution of internal configuration (Ghosh et al. 2001)

An interesting and so-far unexplained phenomenon concerns the precise shape of the axial velocity profiles very close to the downstream stagnation point ($z/a \leq 1$). When plotted in dimensionless form $v_z(z/a;De)/U_s$ the velocity profiles show the existence of a common intersection point which remains unchanged with variations in *De*. In the region very near the sphere ($|\Delta z| < 0.5a$) the velocity is enhanced above that of the corresponding Stokes flow, whereas further from the stagnation point the wake velocity is retarded by elastic effects and is smaller than the value expected for a Newtonian fluid. This effect can also be clearly seen in computations for the analogous planar geometry of a cylinder in a channel (Alves et al. 2001; Fig. 18). It suggests the possibility of a similarity solution for the wake flow region, however this has not been rigorously investigated yet.

2.4.2 Shear-Thinning Viscoelastic Fluids: The Negative Wake

In viscoelastic shear-thinning fluids the magnitudes of both the shear stresses and normal stress differences are more moderate due to molecular entanglement effects. Numerous early experiments investigating the motion behind rising bubbles and sedimenting spheres revealed the existence of a 'negative wake' i.e. an additional recirculating region downstream of the sphere in which the fluid velocity is in the direction opposite to the motion of the sphere and the vorticity is reversed compared to the motion near the sphere (for further details see the historical review in Arigo & McKinley 1998).

The fluids used in the early experiments were typically concentrated polymer solutions Recent experimental measurements of the extensional viscosity and the typical constitutive models used to describe such fluids predict much lower levels of extensional strain-hardening than observed in Boger fluid and possibly even tension-thinning at high *De*. The wake structure is found to be very sensitive to the relative magnitude of such effects. Extensive numerical calculations over the past decade by Jin et al. (1991), Zheng et al. (1991) and Bush (1994)

support the conjecture that both shear-thinning and elasticity are necessary for the formation of a negative wake. In these calculations, four models (Newtonian, Carreau, upper-convected Maxwell and Phan-Thien–Tanner) were used to calculate the velocity field around the sphere. Only when both shear-thinning and elastic effects were present, i.e., in simulations using the PTT model, was a negative wake predicted.

A recurring question has been the precise axial location and extent of the negative wake. Representative LDV velocity profiles in the wake of a highly elastic but shear-thinning 2wt% solution of PPA in glycerin & water (PAA/G/W) are shown in Figure 7. The negative wake results in the development of a stagnation point in the flow and a region of upwardly-directed fluid motion (i.e. away from the sphere) in the wake. Experiments under creeping flow conditions ($Re << 1$) and for radius ratios $0.06 \leq a/R \leq 0.25$ by Arigo & McKinley (1998) showed that the dimensionless velocity profiles are self similar with the stagnation flow located at $z_s/a \approx -3$ and the negative wake extending $-10 \leq z_s/a \leq -3$. However as the dimensionless weight $F_w\lambda/\eta a^2$ of the sphere is increased the shear-thinning in the fluid viscosity leads to inertial effects becoming increasingly important. Since the effective fluid relaxation time and the relative viscosity both decrease with the deformation rate, the Reynolds number $Re = 2\rho U_s a/\eta(\dot{\gamma}_s)$ rises while both the Deborah number $De = \lambda(\dot{\gamma}_s)U_s/a$ and the Elasticity number $El = De/Re$ fall. This leads to the dramatic shift downstream in the position and extent of the wake indicated in Figure 7. Zheng et al. (1991) explored computationally the complex interaction of rheological effects and inertial effects on the wake structure and these experimental observations appear to be consistent with their calculations. The effects of body shape and the interaction of elastic and shear-thinning effects have been extensively documented by Maalouf & Sigli (1984). The early experiments of Bisgaard (1983) exhibited fluctuations in the wake velocity; however, it has not been possible to reproduce these in subsequent investigations.

2.4.3 The Role of Fluid Rheology

Changing the concentration of a polymeric solute and the resulting entanglement density affects both the viscous and elastic properties of a fluid. In experiments it is hard to separate these effects; however, such systematic variations can be investigated computationally. Calculations by Satrape & Crochet (1994) and Harlen et al. (1995) have shown that the formation of a negative wake can be predicted using a constant viscosity, elastic fluid model such as the FENE-CR dumbbell model. The computations shown in Figure 8 demonstrate that

the formation of a negative wake is intimately connected to the extensional properties of the constitutive model, particularly the FENE dumbbell extensibility parameter *L*. For small values of this parameter ($L^2 \sim 10$) a negative wake could be simulated for *De* > 1. As the FENE parameter is increased, and thus the magnitude of the strain-hardening elastic stresses in the wake increase, this negative wake is eliminated.

Regardless of the specific choice of model, both Bush (1994) and Harlen (1997) point out that knowledge of the extensional rheology of the fluid is essential in understanding the evolution of the wake structure. Just as in other complex flow geometries (e.g. flow through an abrupt contraction; White and Baird, 1986), the numerical magnitude of a single dimensionless parameter such as the Deborah (or Weissenberg) number based on viscometric properties of the fluid is insufficient to discriminate between the response of different polymeric fluids or constitutive models. Bush (1994) was able to proceed from a monotonically decaying 'elastic' wake to the formation of a negative wake for the same sphere/cylinder geometry and a 0.25wt% PAA/CS/W solution by changing only the concentration of corn syrup in water from 80% to 30%. Bush attributed this behavior to the interplay between the elasticity of the fluid (quantified by the recoverable shear in viscometric flow) and the magnitude of the elongational stresses in the downstream region. On the basis of these experiments and numerical calculations with the PTT model, Bush suggested that increases in the dimensionless ratio of the Deborah number to the Trouton ratio (De/Tr) led to an upstream shift in the streamlines and ultimately to the formation of a negative wake. Harlen (2001) developed a different criterion from a consideration of the axial force/unit volume $f_z = [\nabla \cdot \boldsymbol{\tau}]_z$ acting on fluid elements in the wake. He argued that the velocity perturbation in the wake of the sphere depends on the relative magnitude of the elongational tensile stresses and the polymeric contribution to shearing stresses in the wake. For high *De* flows of dilute solutions in which the polymer molecules are near full extension, the extensional stresses dominate; however, in concentrated solutions the magnitude of the tensile stresses are dramatically reduced as a result of entanglements and may become of comparable magnitude to the shear stresses. Consideration of the gradients of each contribution to the stress then suggests that the rapid radial variations in the shear stress dominate the slow axial decay of the small tensile stresses and result in a negative wake.

Arigo & McKinley (1998) adapted the criteria described above by using estimates for each term derived from experimental knowledge of the radial and axial extent of the wake. The proposed conditions that are necessary for onset of a negative wake can be conveniently expressed in the following forms:

$$\begin{aligned} &\text{Bush (1994)} && \frac{De}{Tr} \sim \frac{N_1}{\Delta\tau_{ext}} \geq C_1 \\ &\text{Harlen (2001)} && \frac{\eta_p(\dot{\gamma}_s)}{\eta_E} \sim \frac{\tau_{p,rz}}{\Delta\tau_{ext}} \geq C_2\left(\frac{a}{R}\right) \end{aligned} \qquad (12)$$

where the extensional viscosity and the extensional stress difference are related by $\Delta\tau_{ext} = \eta_E\dot{\varepsilon}$ and $\tau_{p,rz}$ is the polymeric contribution to the shear stress.

With the recent advent of filament stretching rheometers it has become possible to accurately measure the transient extensional stress growth in a wide range of polymer solutions. Arigo & McKinley (1998) used a filament stretching device to compare the transient extensional stress growth in the semidilute 0.31 wt% PIB/PB Boger fluid and the 2.0 wt% concentrated PAA/G/W solution utilized in Figs. 5 & 7 respectively. The rheological measurements of the extensional stress growth and the trends observed in the form of the wake structure in each fluid showed that both of these criteria are applicable. From the data presented in Arigo & McKinley it appears that $C_1 \approx C_2 \sim 10^{-2}$.

With experimental results available only for two fluids it is difficult to discern between which mechanism in eq. (12) is primarily responsible for the formation of a negative wake; and whether both conditions are necessary and/or sufficient. It is known that numerical simulations with purely inelastic fluid models such as the Carreau model never show a negative wake (Jin et al. 1991). Furthermore, in steady simple shear flow the upper-convected derivative in the FENE model gives $\tau_{p,xx} = 2(\lambda\dot{\gamma}_s)\tau_{p,yx}$ and so the two criteria are, in fact, inter-related. Interestingly, the Bush criterion involving the magnitude of the dimensionless ratio of normal stress differences in shear and extension has recently been found to be useful in rationalizing trends observed in another fast transient extensional flow: the development and evolution of 'lip vortices' in the flow of elastic fluids into an abrupt contraction (Rothstein & McKinley, 2001). Computational parametric studies investigating the precise form of these criteria that must be satisfied for formation of a negative wake would be most useful.

3. Transient Motion of a Single Sphere

In addition to studying the steady motion of spheres sedimenting in viscoelastic fluids a number of recent investigations have focused on the initial transient motion of a sphere accelerating from rest. This provides a good benchmark for evaluating the efficacy of time-dependent algorithms and provides additional insight into the coupled development of the kinematic structure of the fluid motion in the wake and the elongation of the molecules in the fluid. Once again it is helpful to differentiate between dilute and concentrated polymeric fluids.

3.1 Constant Viscosity Fluids

Tanner & Walters (1992) presented stroboscopic images of a velocity overshoot in a sphere accelerating from rest in a Boger fluid. Becker et al. (1994) subsequently developed a digital imaging system for quantitatively measuring the displacement of the sphere and the time evolution in the settling velocity $U_s(t)$ in a PIB/PB Boger fluid. Jones et al. (1994) used a similar approach and compared the transient response of spheres sedimenting in PAA/CS and PIB/PB Boger fluids.

In transient flows an additional equation of motion for the sphere must be incorporated and the dimensionless time t/λ and the inertia of the sphere now become important, in addition to the parameters in eq. (1). The inertia of the sphere can be characterized by a Stokes number or an Elasticity number E_s based on the particle density rather than the fluid density. This dimensionless number can also be envisioned as a ratio of the polymeric time scale λ and the time scale for inertial acceleration $\Lambda = U^{Stokes}/g \approx 2a^2\rho_s/9\eta_0$. The particle motion following its release under gravity depends on the interaction of the polymeric elasticity, the particle inertia and the viscous damping of the solvent, and a complex oscillatory motion may result as first anticipated by King & Waters (1972). For a Boger fluid the large background solvent viscosity dominates the other effects and a heavily overdamped motion is observed with a single velocity overshoot. If the time scale for inertial acceleration is much smaller than the polymer relaxation time ($E_s >> 1$) then from eq. (4) the sphere initially falls through a quiescent fluid of viscosity η_s. Since the velocity is typically normalized with the steady settling velocity of a sphere in the equivalent Newtonian fluid of viscosity η_0 [i.e. by $U_s(De=0) = U^{Stokes}/K_N(a/R)$] the velocity overshoots by a factor of η_0/η_s (Becker et al. 1994).

As the solvent viscosity is decreased, the amplitude of the overshoot will increase and the rate of damping will decrease until an under-damped oscillatory response is observed. This is demonstrated in Figure 9 by time-dependent FEM calculations using a sphere of constant density and radius (and hence constant dimensionless weight) together with the Oldroyd-B constitutive model and two different solvent viscosity ratios (Bodart & Crochet, 1994). These calculations also show graphically that the magnitude of the initial velocity overshoot and the subsequent damped oscillations vary significantly with the constraining effects of the container walls.

Experiments by Arigo & McKinley (1997) suggest that the effects of solvent viscosity and bounding walls can be incorporated, at least approximately, into the solution presented by King & Waters for an unbounded linear viscoelastic fluid by replacing the Stokes settling

velocity by the value expected from eq. (6). In the limit that unsteady effects in the fluid are negligibly small (such that $\rho/\rho_s << 1$), the resulting equation for the trajectory of the sphere becomes (in dimensionless form)

$$\frac{U_s(t)}{\left(U^{Stokes}/K_N\right)} = 1 + \frac{E_K\sqrt{1-\eta_s/\eta_0}}{\omega_K}\exp\left(-\varepsilon_K\, t/\lambda\right)\sin\left(\omega_K t/\lambda - \phi_K\right) \tag{13}$$

where $E_K = E_S K_N(a/R)$ is the wall-enhanced Elasticity number of the sphere; $\varepsilon_K = \frac{1}{2}\left(1 + E_K\eta_s/\eta_0\right)$ is the dimensionless damping rate, $\omega_K = \sqrt{{E_K}^2 - {\varepsilon_K}^2}$ is the dimensionless oscillation frequency and $\phi_K = \arctan\left(\lambda\omega_K/(E_K - \varepsilon_K)\right)$ satisfies the initial condition that $U_s(0) = 0$. For the case of a Maxwell fluid with $E_S >> \left(\lambda\varepsilon\right)^2$ the oscillation frequency varies as $\omega \sim \sqrt{\eta_0/(\lambda\rho_s a^2)}$ however for real fluids the effects of the solvent viscosity and the presence of the walls cannot be neglected. This sensitivity of both the damping rate and oscillation frequency to the solvent viscosity and the proximity of the outer channel walls is demonstrated in Fig 9 and is also captured in the expression above.

All of the calculations described above involved constitutive models with a single characteristic relaxation time. However since the experiments involve rapid accelerations the shorter relaxation modes and the precise form of the viscometric functions and the extensional rheology of the fluid play a very important role in controlling the trajectory of the sphere. Such effects have been explored in numerical calculations by Rasmussen (Becker et al. 1994; Rasmussen & Hassager, 1996) and multimode computational studies by Rajagopalan et al (1995). Accurate time–dependent numerical algorithms for integral constitutive models have also been described by Rasmussen (1999) & Peters et al. (2000).

3.2 Viscoelastic Shear Thinning Fluids

Transient calculations by Zheng & Phan-Thien (1992) using the UCM model showed that if the fluid elasticity becomes very large the amplitude of the oscillations can grow large enough that the accelerating sphere reverses its direction briefly and travels up the tube in the opposite direction to gravity. It is difficult to construct a UCM-like fluid experimentally: in ideal elastic fluids, video-imaging experiments and simulations with the Oldroyd-B model show that such effects are damped by the large solvent viscosity (typically $\eta_s/\eta_0 \geq 0.5$); conversely in highly elastic concentrated solutions the solvent contribution to the viscosity can be made much smaller but shear-thinning effects also become important. Transient simulations showing the evolution of the wake in such a system have yet to be performed. Harlen et al. (1995) show that a negative

wake develops at early times in the transient evolution of a wake in an Oldroyd-B fluid when the tensile stresses are small. This is consistent with the criteria in eq. (12). As the sphere approaches steady state, this temporary negative wake disappears as the molecules in the wake become more highly oriented and elongated, and the large extensional stresses dominate the flow in the wake.

A sequence of DPIV images showing the motion of an aluminum sphere and the surrounding velocity field in a 2 wt% PAA/CS/W fluid are presented in Fig. 10. A very large velocity overshoot ($U_{\max}(t)/U_s \sim 7$) occurs at short times and is governed by the linear viscoelastic response of the fluid. The sphere then reverses directions briefly before resuming its sedimentation at longer times. LDV and DPIV images show that negative wake develops only after large strains ($\gamma_s = \int \dot{\gamma}_s(t)dt \sim 5$) have accumulated and is thus associated with the nonlinear viscoelastic properties of the fluid.

In addition to the initial transient acceleration from rest under a constant force, a number of theoretical studies have considered other classes of unsteady motions. Ramkissoon & Shifang (1993) considered cases of constant acceleration and exponentially decreasing acceleration in a generalized Maxwell model. Mei et al. (1996) considered the small amplitude oscillatory motion of a sphere in a cylinder containing linear viscoelastic fluid and computed the real and imaginary contributions to the time-varying drag force. On the basis of these calculations they suggested a method for determining the constitutive parameters characterizing the linear viscoelastic properties of the fluid from measurements of the unsteady drag on the sphere. Such rheological techniques are particularly useful when the spherical particles are small enough that Brownian forces become important enough to provide the random oscillatory forcing (i.e. when $k_B T/a \sim 6\pi\eta_0 U a$). The fluctuations in the trajectory of the sphere can then be used as a microrheometric probe of the suspending medium. By following the two-dimensional correlations in the particle position it is possible to obtain a measure of the viscoelastic properties within very small samples of complex fluid materials such as cellular cytoplasm and other biopolymer solutions. Further details of the analysis required can be found in the recent study by Levine & Lubensky (2001).

4. More Complex Interactions

By understanding the important role of the fluid extensional rheology on the form and spatial extent of the viscoelastic wake structures behind a sedimenting sphere, one can begin to understand the driving forces governing the interactions in more complex problems such as the

aggregation or dispersion of multiple particles (see for example the classic work of Riddle et al. 1977). Joseph and co-workers have reviewed early work in this area (Liu & Joseph, 1993) and extensively investigated these phenomena in subsequent publications. Here we briefly describe some recent developments in this area:

4.1 Interactions between a Sphere and a Wall

The simplest non-axisymmetric configuration to realize is the sedimentation of a sphere near a single planar wall. As a result of the symmetry and reversibility of the Stokes equations, migration towards or away from the wall is not possible in creeping flow through a Newtonian fluid; however it should be noted that if one considers a sphere settling in a cylindrical tube but offset from the centerline by a distance $0 < \delta < (R - a)$ the steady settling speed of the sphere may vary non-monotonically with the extent of the lateral offset (Happel & Brenner, 1964). In creeping flow through a viscoelastic fluid, particles are observed experimentally to experience a 'negative lift force' (i.e. towards the wall) and an 'anomalous rotation' in the reverse direction to the anticipated rolling motion (Liu et al. 1993). In experiments investigating such phenomena the presence of the three additional container walls must always be taken into account because of the slow ($1/r$) decay of velocity perturbations in low Reynolds number flows. For example, Liu et al. (1993) use very narrow containers with a/R = 0.45, 0.15 and 0.125 and significant effects from the far wall should also be expected. In subsequent experiments, Becker et al. (1996) still observed an elastic drift towards the wall and anomalous rotation even in much large containers. These authors also used an ordered fluid expansion together with the reciprocal theorem to show that weak elastic effects (up to second order in *De*) can reduce the rotation rate observed in a Newtonian fluid but cannot give rise to the anomalous rotation observed experimentally. Weak elastic effects were found to result in a lift force away from the wall in contrast to the experimental observations. Two dimensional simulations incorporating elasticity and inertia by Feng et al. (1996) of a circular disk falling near a plane wall were able to qualitatively capture many features of the anomalous rotation and elastic lift. With recent advances in computational capabilities, full three-dimensional and quantitative studies of this phenomena have become possible. Binous & Phillips (1996b) have presented a Stokesian dynamics algorithm for simulating a suspension of FENE dumbbells and more recently Singh & Joseph (2000) used a finite element method to study sedimentation in viscoelastic fluids described by the Oldroyd-B fluid. Comparison of 2D and 3D simulations show that the attractive force towards the wall only arises in the three-dimensional flow

4.2 Interactions between Two Spheres

When two spheres fall through a viscoelastic liquid the wakes behind the objects can interact. Bot et al. (1998) considered the interactions between two identical spheres sedimenting along their line of centers through a constant viscosity elastic liquid and found that there is a stable separation distance between the spheres. An observer traveling in the reference frame of the trailing sphere (sphere 2) experiences an approaching fluid velocity of magnitude $U_s - v_z^{(1)}(z; De, a/R)$ which is lower than that observed in the corresponding Newtonian fluid due to the slow elastic decay of the velocity in the wake of the lead sphere (sphere 1). Here the subscripts (1) and (2) correspond to the leading and trailing spheres respectively. The trailing sphere thus sediments faster than the lead sphere. However as it gets closer to the first sphere, the polymer molecules entering the biaxial stagnation flow near the nose of the trailing sphere retain an increasing fraction of the orientation induced in the transient extensional wake flow behind the leading sphere. This 'pre-conditioning' leads to enhanced viscoelastic stresses near the second sphere and an additional elastic contribution to the total drag. When these two competing effects balance, the spheres sediment at constant separation distance. As we have shown in §2.3 the wake structure is a very sensitive function of both the Deborah number and the radius ratio; it is thus perhaps not surprising that the stable separation distance measured by Bot et al. (1998) also increases with De .

By contrast, in a concentrated polymer solution with a negative wake of the form depicted in Fig 8 there is no stable separation distance. Trailing spheres at axial separations beyond the free stagnation point located at z_{stag} are retarded by the axial outflow and sediment more slowly; whereas spheres at smaller separations are entrained by the negative wake and attracted towards the leading sphere. They then aggregate and fall as a doublet. This can lead to the formation of chains of particles (Liu & Joseph, 1993).

When the two spheres fall in a side by side configuration the modifications to the flow around the two bodies can result in an attractive force which causes them to migrate towards each other. A sequence of photographic images of this attraction is shown in Fig 11 (Joseph et al. 1994). As the spheres approach each other they rotate end-on to the flow and fall as a doublet. By contrast, using the same experimental configuration and a viscous Newtonian fluid Joseph & coworkers found the two spheres repelled each other. The experiments of Joseph et al. were all performed in concentrated polymer solutions which we expect to have limited extensional viscosities and a negative wake structure as shown in Figs. 7 & 8; however, the driving forces for aggregation and rotation appear to be present even at moderate *De* and can thus be described at least qualitatively by simpler quasilinear constitutive equations. Physical arguments for such

migrations which are based on the second order fluid and the local pressures and elastic stresses near the forward and rear stagnation points have been discussed by Joseph & Feng (1996). Two dimensional simulations for pairs of circular and elliptical particles and the Oldroyd-B model have been presented by Feng et al. (1996) and Huang et al. (1998) respectively. The first complete three-dimensional simulation of this aggregation process in a suspension of FENE dumbbells was presented by Binous & Joseph (1999a). A representative trajectory at $De = 3$ with a low finite extensibility ($L^2 = 10$) is shown in Figure 11b. The pair of spheres are initially released side by side but this configuration is unstable. The larger tensile stress in the wake of the trailing sphere exerts a couple on the pair which leads to a progressive rotation. The slow dynamics of the process are clear in both Figs 11(a) & 11(b); the simulations show that the particles fall by 800 particle radii over a period of 150 time constants as they rotate through 90˚. The weak lateral drift shown in the experiments when the composite slender body is inclined at intermediate angles is also realized in the computations.

4.3 Multiple Spheres & Viscoelastic Suspensions

One of the ultimate goals of research into sedimentation is to understand the dynamics of suspensions of spherical particles in viscoelastic matrix fluids. As the number of interacting particles increases, the problem complexity increases correspondingly but with the advances in experimental and computational techniques over the past decade significant progress in our understanding has been made. Such topics are really the subject of a separate review but some of the key phenomena observed can be rationalized in terms of the insight gained in studies with single spheres.

In dilute suspensions (with volume fractions typically $\phi \leq 10\%$), one of the most important phenomena is recognized to be shear-induced migration and the formation of larger scale structures such as chains of particles. Van den Brule & Gheissary (1993) explored the interactions between three identical spheres and also showed that a background shear flow (generated in a circular Couette geometry) could dramatically affect the measured sedimentation velocity due to changes in the effective state of stress in the fluid around the particles. The tendency for two interacting spheres in an elastic liquid to also migrate laterally was shown in Fig.11. In flowing suspensions this can lead to significant shear-induced migration (Tehrani 1996). The formation of chains and aggregates under such shearing conditions has been extensively investigated by Feng & Joseph (1996). A sequence of images depicting this phenomena are shown in Figure 13. Although the extensional viscosity of the test liquid (2 wt%

PEO/W) was not characterized, we may confidently expect that the limited extensional viscosity and shear-thinning in the viscometric properties lead to the criteria in eq. (12) being satisfied so that a negative wake structure develops. Additional spheres moving on neighboring streamlines in the vicinity of the recirculating wake are then swept towards the rear stagnation point and accumulate into chains. On longer time-scales these chains form concentric rings with a characteristic wavelength on the scale of the gap *H*. With the ability to now simulate three-dimensional time-dependent motions of bodies in viscoelastic fluids an important next step is to compute the effective 'capture radii' for this shear-induced aggregation as a function of the parameters in the constitutive model.

In concentrated suspensions ($\phi \geq 10\%$) the ability to form, or indeed even to image, shear-induced structures is much harder, and experiments have instead focused on the effective rheological properties of the suspension. Under conditions of equivalent imposed shear stress it has been shown (Ohl & Gleissle, 1992) that the first normal stress difference in a highly filled suspension is reduced, and the second normal stress difference enhanced, compared to that of the pure viscoelastic matrix fluid. The progressive variation in these viscometric functions with volume fraction of filler and imposed shear stress appear to be intimately connected (Mall-Gleissle et al. 2001). The ability to systematically vary the viscoelastic properties of a filled polymeric material is important in controlling other non-Newtonian phenomena that arise during processing such as the magnitude of die swell (Markovic et al. 2000) and the critical conditions for onset of elastic instabilities (Kazatchkov et al. 2000). Computational studies of the effective linear viscoelastic properties (Schaink et al. 2000) and nonlinear viscometric properties (Patankar & Hu, 2001) of filled elastic fluids are just beginning and should be an area of great progress in the near future.

5. Conclusions

The substantial advances that have been made over the last decade in this viscoelastic benchmark problem has resulted from complementary developments in each of the following areas:

- experimental tools for quantitative imaging of the complex flow near the sphere with high spatial and temporal resolution,
- improved rheological techniques for characterizing viscoelastic properties of the test fluids such as the first normal stress difference and the transient extensional viscosity over a wide range of deformation rates,

- steady and time-dependent numerical techniques for computation to high *De* which are stable and mesh-convergent.

As we have tried to show in this review, significant progress has been made, however challenges still remain: particularly in the areas of particle-particle interactions and analysis of flow stability. In addition, the bulk of the studies we have reviewed have focused on homogeneous well-mixed polymer solutions. In many experimental systems there are additional molecular-level phenomena such as the well-known 'time-effect' (Walters & Tanner, 1992) which have yet to be quantitatively explained. These effects lead to systematic variations between the sedimentation velocity of successively-dropped spheres possibly due to either stress-induced migration of molecules away from the wake, or from the disruption of equilibrium networks of hydrogen bonds or other secondary structures (Ambeshkar & Mashelkar 1990). Agarwal et al. (1994) provide an extensive review of the literature in this area and Gheissary & van den Brule (1996) present measurements of very extravagant 'time-effects' during the dropping of successive spheres through a gel-like solution of Carbopol (polyacrylic acid).

There are also other fluids which exhibit viscoelastic behavior such as physical gels and polymeric surfactant systems which have been less well-studied and which can exhibit even more complex behavior during sedimentation. As an example we show in Fig. 13 a sequence of digital video images of a sphere sedimenting through a worm-like surfactant solution of 9 mM cetyltrimethylammonium bromide/sodium salicylate (CTAB/NaSal). The images are separated by a fixed time increment of 0.26 seconds but it is clear that the sphere velocity is not constant. As shown in the figure the velocity in fact continuously fluctuates in a complex manner. The fluid is well-mixed and this fluctuating motion appears to be the result of a stress-induced instability in the micellar network which leads to dramatic changes in the fluid viscoelasticity (Jayaraman & Belmonte, 2001). Qualitatively similar observations were noted by Mollinger et al. (1999) in hydroy propyl guar (HPG) gels for sphere/tube ratios $a/R \geq 0.25$.

Such instabilities appear to be common in viscoelastic surfactant systems and may be due to the 'gel-like' character: i.e. a very high elasticity under small amplitude deformations, but a very strong shear-thinning during larger strains. In addition, extensional viscosity measurements for such fluids show a very limited extensional stress increase followed by a catastrophic network rupture (McKinley, 2000). All of these material responses will play a role in the complex flow field near a sedimenting sphere. The growing importance of worm-like surfactants and associative polymer solutions as rheology modifiers and thickeners in highly-filled materials such as foods, paints and other consumer products suggests that the study of sedimentation in these gel-like fluids will be an increasingly active area over the coming decade.

Acknowledgments

I would like to thank Prof. Mark Arigo and Dr. Oliver Harlen for numerous illuminating discussions over the years on the subject of sedimentation phenomena in viscoelastic media.

6. Bibliography

Agarwal, U.S., Dutta, A. and Mashelkar, R.A., Migration of Macromolecules under Flow: The Physical Origin and Engineering Implications, *Chem. Eng. Sci.*, **498**(11), (1994), 1693-1717.

Alves, M.A., Pinho, F.T. and Oliveira, P.J., The Flow of Viscoelastic Fluids Past a Cylinder: Finite-Volume High-Resolution Methods, *J. Non-Newt. Fluid Mech.*, **97**(2-3), (2001), 207-232.

Ambeskar, V.D. and Mashelkar, R.A., On the role of stress-induced migration on time-dependent terminal velocities of falling spheres, *Rheol. Acta*, **29**, (1990), 182-191.

Arigo, M.T. and McKinley, G.H., The Effects of Viscoelasticity on the Transient Motion of a Sphere in a Shear-Thinning Fluid, *J. Rheol.*, **41**(1), (1997), 103-128.

Arigo, M.T. and McKinley, G.H., An experimental investigation of negative wakes behind spheres settling in a shear-thinning viscoelastic fluid, *Rheol. Acta*, **37**(4), (1998), 307-327.

Arigo, M.T., Rajagopalan, D.R., Shapley, N.T. and McKinley, G.H., Sedimentation of a Sphere Through an Elastic Fluid: Part I Steady Motion, *J. Non-Newt. Fluid Mech.*, **60**, (1995), 225-258.

Baaijens, F.P.T., Mixed Finite Element Methods for Viscoelastic Flow Analysis: A Review, *J. Non-Newt. Fluid Mech.*, **79**(2-3), (1998), 361-385.

Baaijens, H.P.W., Peters, G.W.M., Baaijens, F.P.T. and Meijer, H.E.H., Viscoelastic flow past a confined cylinder of a polyisobutylene solution, *J. Rheol.*, **39**(6), (1995), 1243-1277.

Becker, L., McKinley, G.H., Rasmussen, H.K. and Hassager, O., The Unsteady Motion of a Sphere in a Viscoelastic Fluid, *J. Rheol.*, **38**(2), (1994), 377-403.

Becker, L., McKinley, G.H. and Stone, H.A., Sedimentation of a Sphere Near a Plane Wall: Weak Non-Newtonian and Inertial Effects, *J. Non-Newt. Fluid Mech.*, **63**, (1996), 201-233.

Binous, H. and Phillips, R.J., Dynamic simulation of one and two particles sedimenting in viscoelastic suspensions of FENE dumbbells, *J. Non-Newt. Fluid Mech.*, **83**(1-2), (1999), 93-130.

Binous, H. and Phillips, R.J., The effect of sphere-wall interactions on particle motion in a viscoelastic suspension of FENE dumbbells, *J. Non-Newt. Fluid Mech.*, **85**(1), (1999), 63-92.

Bird, R.B., Armstrong, R.C. and Hassager, O., Dynamics of Polymeric Liquids. Volume 1: Fluid Mechanics, Vol. 1, 2nd Edition, Wiley Interscience, New York, 1987.

Bisgaard, C., Velocity Fields Around Spheres and Bubbles Investigated by Laser-Doppler Anemometry, *J. Non-Newt. Fluid Mech.*, **12**, (1983), 283-302.

Bodart, C. and Crochet, M.J., The time-dependent flow of a Viscoelastic Fluid Around a Sphere, *J. Non-Newt. Fluid Mech.*, **54**, (1994), 303-329.

Boger, D.V., A Highly Elastic Constant-Viscosity Fluid, *J. Non-Newt. Fluid Mech.*, **3**, (1977/78), 87-91.

Bot, E.T.G., Hulsen, M.A. and van den Brule, B.H.A.A., The motion of Two Spheres Falling Along Their Line of Centers in a Boger Fluid, *J. Non-Newt. Fluid Mech.*, **79**, (1998), 191-212.

Brandrup, H. and Immergut, E.H., Polymer Handbook, Wiley, New York, 1997.

Brown, R.A., Szady, M.J., Northey, P.J. and Armstrong, R.C., On the Numerical Stability of Mixed Finite-Element Methods for Viscoelastic Flows Governed by Differential Constitutive Equations, *Theoret. Comput. Fluid Dynamics*, **5**, (1993), 77-106.

Brown, R.A. and McKinley, G.H., Report on the VIIIth International Workshop on Numerical Methods in Viscoelastic Flows, *J. Non-Newt. Fluid Mech.*, **52**, (1994), 407-413.

Bush, M.B., The Stagnation Flow Behind a Sphere, *J. Non-Newt. Fluid Mech.*, **49**, (1993), 103-122.

Bush, M.B., On The Stagnation Flow Behind a Sphere in a Shear-Thinning Viscoelastic Liquid, *J. Non-Newt. Fluid Mech.*, **55**, (1994), 229-247.

Ceylan, K., Herdem, S. and Abbasov, T., A theoretical model for estimation of drag force in the flow of non-Newtonian fluids around spherical solid particles, *Powder Technology*, **103**(3), (1999), 286-291.

Chauviere, C. and Owens, R.G., How accurate is your solution? Error indicators for viscoelastic flow calculations, *J. Non-Newt. Fluid Mech.*, **95**(1), (2000), 1-33.

Chhabra, R.P., Bubbles, Drops and Particles in Non-Newtonian Fluids, CRC Press, Boca Raton, 1993.

Chhabra, R.P., Tiu, C. and Uhlherr, P.H.T., A Study of Wall Effects on the Motion of a Sphere in Viscoelastic Fluids, *Can. J. Chem. Eng.*, **59**, (1981), 771-775.

Chhabra, R.P. and Uhlherr, P.H.T., The Influence of Fluid Elasticity on Wall Effects for Creeping Sphere Motion in Cylindrical Tubes, *Can. J. Chem. Eng.*, **66**, (1988), 154-157.

Chhabra, R.P., Uhlherr, P.H.T. and Boger, D.V., The Influence of Elasticity on the Drag Coefficient for Creeping Flow around a Sphere, *J. Non-Newt. Fluid Mech.*, **6**, (1980), 187-199.

Chilcott, M.D. and Rallison, J.M., Creeping Flow of Dilute Polymer Solutions Past Cylinders and Spheres, *J. Non-Newt. Fluid Mech.*, **29**, (1988), 381-432.

Degand, E. and Walters, K., On the Motion of a Sphere Falling Through an Elastic Liquid Contained in a Tight-Fitting Cylindrical Container, *J. Non-Newt. Fluid Mech.*, **57**(1), (1995), 103-115.

Delvaux, V. and Crochet, M.J., Numerical Prediction of Anomalous Transport Properties in Viscoelastic Flow, *J. Non-Newt. Fluid Mech.*, **37**, (1990), 297-315.

Doi, M., Introduction to Polymer Physics, Clarendon, Oxford, 1997.

Doyle, P. and Shaqfeh, E.S.G., Dynamic Simulation of Freely-Draining, Flexible Bead-Rod Chains: Start-Up of Extensional & Shear Flow, *J. Non-Newt. Fluid Mech.*, **76**(1-3), (1998), 79-110.

Doyle, P., Shaqfeh, E.S.G., McKinley, G.H. and Spiegelberg, S.H., Relaxation of Dilute Polymer Solutions Following Extensional Flow, *J. Non-Newt. Fluid Mech.*, **76**(1-3), (1998), 79-110.

Fabris, D., Muller, S.J. and Liepmann, D., Wake measurements for flow around a sphere in a viscoelastic fluid, *Phys. Fluids*, **11**(12), (1999), 3599-3612.

Fan, Y.R., Tanner, R.I. and Phan-Thien, N., Galerkin/least-square finite-element methods for steady viscoelastic flows, *J. Non-Newt. Fluid Mech.*, **84**(2-3), (1999), 233-256.

Feng, J., Huang, P.Y. and Joseph, D.D., Dynamic Simulation of Sedimentation of Solid Particles in an Oldroyd-B fluid, *J. Non-Newt. Fluid Mech.*, **63**(1996), (1996), 63-88.

Feng, J. and Joseph, D.D., The motion of solid particles suspended in viscoelastic liquids under torsional shear, *J, Fluid Mech.*, **324**, (1996), 199-222.

Gervang, B., Davies, A.R. and Phillips, T.N., On the Simulation of Viscoelastic Flow Past a Sphere using Spectral Methods, *J. Non-Newt. Fluid Mech.*, **44**, (1992), 281-306.

Gheissary, G. and van den Brule, B.H.A.A., Unexpected Phenomena observed in particle settling in non-Newtonian Media, *J. Non-Newt. Fluid Mech.*, **67**, (1996), 1-18.

Ghosh, I., McKinley, G.H., Brown, R.A. and Armstrong, R.C., Deficiencies of FENE Dumbbell Models in Describing the Rapid Stretching of Dilute Polymer Solutions, *J. Rheol.*, **45**(3), (2001), 721-758.

Happel, J. and Brenner, H., Low Reynolds Number Hydrodynamics: Mechanics of Fluids and Transport Processes, Martinus Nijhoff, Dordrecht, 1973.

Harlen, O.G., High-Deborah-Number Flow of a Dilute Polymer Solution Past a Sphere Falling Along the Axis of a Cylindrical Tube, *J. Non-Newt. Fluid Mech.*, **37**, (1990), 157-173.

Harlen, O.G., The Negative Wake Behind a Sedimenting Sphere, *J. Non-Newt. Fluid Mech.*, (2001), in preparation.

Harlen, O.G., Rallison, J.M. and Szabo, P., A Split Lagrangian-Eulerian Method For Simulating Transient Viscoelastic Flows, *J. Non-Newt. Fluid Mech.*, **60**(1), (1995), 81-104.

Harrison, G.M., Lawson, N.J. and Boger, D.V., The Measurement of the Flow Around a Sphere Settling in a Rectangular Box using 3-Dimensional Particle Image Velocimetry, *Chem. Eng. Commun.*, (2001), submitted.

Hassager, O., Working Group on Numerical Techniques, *J. Non-Newt. Fluid Mech.*, **29**, (1988), 2-5.

Hernández Cifre, J.G. and de la Torre, J.G., Simulation of Polymers in Dilute Solution under Elongational Flow, *J. Non-Cryst. Solids*, **235-237**, (1998), 717-722.

Huang, P.Y. and Feng, J., Wall Effects on the Flow of Viscoelastic Fluids Around a Circular Cylinder, *J. Non-Newt. Fluid Mech.*, **60**, (1995), 179-198.

Huang, P.Y., Hu, H.H. and Joseph, D.D., Direct simulation of the sedimentation of elliptic particles in Oldroyd-B fluids, *J. Fluid Mech.*, **362**, (1998), 297-325.

Ilic, V., Tullock, D., Phan-Thien, N. and Graham, A.L., Translation and Rotation of Spheres Settling in Square and Circular Conduits: Experiments and Numerical Predictions, *Int. J. Multiphase Flow*, **18**(6), (1992), 1061-1075.

Jayaraman A. and Belmonte, A., Presentation at the Annual Meeting of the Society of Rheology, Hilton Head, Feb 2001.

Jin, H., Phan-Thien, N. and Tanner, R.I., A Finite Element Analysis of the Flow Past a Sphere in a Cylindrical Tube: PTT Fluid Model, *Comp. Mech.*, **8**, (1991), 409-422.

Jones, W.M., Price, A.H. and Walters, K., The Motion of a Sphere Falling Under Gravity in a Constant-Viscosity Elastic Liquid, *J. Non-Newt. Fluid Mech.*, **53**, (1994), 175-196.

Joseph D.D, Feng J. 1996. A note on the forces that move particles in a second-order fluid. *J. Non-Newt. Fluid Mech*. 64(2-3): 299-302.

Joseph, D.D., Liu, Y.F., Poletto, M. and Feng, J., Aggregation and Dispersion of Spheres falling in Viscoelastic Liquids, *J. Non-Newt. Fluid Mech.*, **54**, (1994), 45-86.

Kazatchkov, I.B., Yip, F. and Hatzikiriakos, S.G., The effect of boron nitride on the rheology and processing of polyolefins, *Rheol. Acta*, **39**(6), (2000), 583-594.

King, M.J. and Waters, N.D., The Unsteady Motion of a Sphere in an Elastico-Viscous Liquid, *J. Phys. D: Appl. Phys.*, **5**, (1972), 141-150.

Larson, R.G., Hu, H., Smith, D.E. and Chu, S., Brownian dynamics simulations of a DNA molecule in an extensional flow field, *J. Rheol.*, **43**(2), (1999), 267-304.

Leslie, F.M. and Tanner, R.I., The Slow Flow of a Viscoelastic Liquid Past a Sphere, *Quart. J. Mech. Appl. Math.*, **14**, (1961), 36-48.

Levine, A.J. and Lubensky, T.C., Response function of a sphere in a viscoelastic two-fluid medium, *Phys. Rev. E*, **6304**(4), (2001), 1510-.

Li, L. and Larson, R.G., Excluded Volume Effects on the Birefringence and Stress of Dilute Polymer Solutions in Extensional Flow, *Rheol. Acta*, **39**(5), (2001), 419-427.

Li, L., Larson, R.G. and Sridhar, T., Brownian Dynamics Simulations of Dilute Polystyrene Solutions, *J. Rheol.*, **44**(2), (2000), 291-323.

Liu, A., Viscoelastic Flow of Polymer Solutions Around Arrays of Cylinders: Comparison of Experiment & Theory, *Ph.D. Thesis,* MIT, (1997).

Liu, Y.J. and Joseph, D.D., Sedimentation of Particles in Polymer Solutions, *J. Fluid Mech.*, **255**, (1993), 565-595.

Liu, Y.J., Nelson, J., Feng, J. and Joseph, D.D., Anomalous Rolling of Spheres Down an Inclined Plane, *J. Non-Newt. Fluid Mech.*, **50**, (1993), 305-329.

Lunsmann, W.J., Genieser, L., Brown, R.A. and Armstrong, R.C., Finite Element Analysis of Steady Viscoelastic Flow Around a Sphere: Calculations with Constant Viscosity Models, *J. Non-Newt. Fluid Mech.*, **48**, (1993), 63-99.

Maalouf, A. and Sigli, D., Effects of Body Shape and Viscoelasticity on the Slow Flow around an Obstacle, *Rheol. Acta*, **23**, (1984), 497-507.

Mackay, M.E. and Boger, D.V., An Explanation of the Rheological Properties of Boger Fluids, *J. Non-Newt. Fluid Mech.*, **22**, (1987), 235-243.

Mall-Gleissle, S., Gleissle, W., McKinley, G.H. and Buggisch, H., The Normal Stress Behavior of Suspensions with Viscoelastic Matrix Fluid, *Rheol. Acta*, (2001), in press.

Markovic, M.G., Choudhury, N.R., Dimopoulos, M., Matisons, J.G., Dutta, N.K. and Bhattacharya, A.K., Rheological behavior of highly filled ethylene propylene diene rubber compounds, *Polym. Eng. & Sci.*, **40**(5), (2000), 1065-1073.

McKinley, G.H., The Nonlinear Dynamics of Viscoelastic Flow in Complex Geometries, *Ph.D. Thesis,* M.I.T., (1991).

McKinley, G.H., "A Decade of Filament Stretching Rheometry", Proceedings of the. XIIIth Int. Cong. Rheology,Vol.1, D. M. Binding, N. E. Hudson, J. Mewis, J.-M. Piau, C. J. S. Petrie, P. Townsend, M. H. Wagner and K. Walters (ed.), British Society of Rheology, Cambridge (UK), 2000, 15-22.

McKinley, G.H., Armstrong, R.C. and Brown, R.A., The Wake Instability in Viscoelastic Flow Past Confined Circular Cylinders, *Phil. Trans. R. Soc. Lond. A*, **344**, (1993), 265-304.

McKinley, G.H. and Sridhar, T., Filament Stretching Rheometry of Complex Liquids, *Ann. Rev. Fluid Mech.*, **34**, (2002), to appear.

Mei, R.W., Xiong, J. and TranSonTay, R., Motion of a sphere oscillating at low Reynolds numbers in a viscoelastic-fluid-filled cylindrical tube, *J. Non-Newt. Fluid Mech.*, **66**(2-3), (1996), 169-192.

Mena, B., Manero, O. and Leal, L.G., The Influence of Rheological Properties on the Slow Flow Past Spheres, *J. Non-Newt. Fluid Mech.*, **26**, (1987), 247-275.

Missirlis, K.A., Assimacopoulos, D., Mitsoulis, E. and Chhabra, R.P., Wall effects for Motion of Spheres in Power-Law Fluids, *J. Non-Newt. Fluid Mech.*, **96**(3), (2001), 459-471.

Mitsoulis, E., Effect of rheological properties on the drag coefficient for creeping motion around a sphere falling in a tightly-fitting tube, *J. Non-Newt. Fluid Mech.*, **74**(1-3), (1998), 263-283.

Mollinger, A.M., Cornelissen, E.C. and van den Brule, B.H.A.A., An Unexpected Phenomenon Observed in Particle Settling: Oscillating Falling Spheres, *J. Non-Newtonian Fluid Mech.*, **86**(3), (1999), 389-393.

Oh, J.H. and Lee, S.J., A Rheological Study on the Viscoelastic Flow Past Spheres in a Cylinder, *J. Mater. Process. and Manufacturing Sci.*, **1**, (1992), 3-15.

Ohl, N. and Gleissle, W., The Second Normal Stress Difference for Pure and Highly Filled Viscoelastic Fluids, *Rheol. Acta*, **31**, (1992), 294-305.

Owens, R.G. and Phillips, T.N., Steady viscoelastic flow past a sphere using spectral elements, *Int. J. Numer. Methods Eng.*, **39**(9), (1996), 1517-1534.

Öztekin, A., Alakus, B. and McKinley, G.H., Stability of Planar Stagnation Flow of a Highly Viscoelastic Fluid, *J. Non-Newt. Fluid Mech.*, **72**(1), (1997), 1-30.

Pakdel, P. and McKinley, G.H., Digital Particle Imaging Velocimetry of Viscoelastic Fluids, *A.I.Ch.E. J.*, **43**(2), (1997), 289-302.

Patankar, N.A. and Hu, H.H., Rheology of a Suspension of Particles in Viscoelastic Fluids, *J. Non-Newt. Fluid Mech.*, **96**(2-3), (2001), 427-443.

Peters, E., Hulsen, M.A. and van den Brule, B., Instationary Eulerian viscoelastic flow simulations using time separable Rivlin-Sawyers constitutive equations, *J. Non-Newt. Fluid Mech.*, **89**(1-2), (2000), 209-228.

Rajagopalan, D.R., Arigo, M.T. and McKinley, G.H., Sedimentation of a Sphere Through an Elastic Fluid: Part II Transient Motion, *J. Non-Newt. Fluid Mech.*, **65**, (1996), 17-46.

Rallison, J.M., Dissipative Stresses in Dilute Polymer Solutions, *J. Non-Newt. Fluid Mech.*, **68**, (1997), 61-83.

Ramkissoon, H. and Shifang, H., Unsteady Motion of a Sphere in an Elastico-Viscous Fluid, *Int. J. Engng Sci.*, **31**(1), (1993), 19-26.

Rasmussen, H.K., Time-dependent finite-element method for the simulation of three-dimensional viscoelastic flow with integral models, *J. Non-Newt. Fluid Mech.*, **84**(2-3), (1999), 217-232.

Rasmussen, H.K. and Hassager, O., On the sedimentation velocity of spheres in a polymeric liquid, *Chem. Eng. Sci.*, **51**(9), (1996), 1431-1440.

Renardy, M., Asymptotic Structure of the Stress Field in Flow Past a Cylinder at high Weissenberg Number, *J. Non-Newt. Fluid Mech.*, **90**(1), (2000), 13-23.

Riddle, M.J., Narvaez, C. and Bird, R.B., Interactions Between Two Spheres Falling Along Their Line of Centers in a Viscoelastic Fluid, *J. Non-Newt. Fluid Mech.*, **2**, (1977), 23-35.

Rodrique, D., de Kee, D. and Chan Man Fong, C.F., The Slow Motion of a Spherical Particle in a Carreau Fluid, *Chem. Eng. Commun.*, **154**, (1996), 203-215.

Ryskin, G., Calculation of the Effect of Polymer Additive in a Converging Flow, *J. Fluid Mech.*, **178**, (1987), 423-440.

Satrape, J.V. and Crochet, M.J., Numerical Simulation of the Motion of a Sphere in a Boger fluid, *J. Non-Newt. Fluid Mech.*, **55**, (1994), 91-111.

Schaink, H.M., Slot, J.M., Jongschaap, R.J.J. and Mellema, J., The rheology of systems containing rigid spheres suspended in both viscous and viscoelastic media, studied by Stokesian dynamics simulations, *J. Rheol.*, **44**(3), (2000), 473-498.

Singh, P. and Joseph, D.D., Sedimentation of a sphere near a vertical wall in an Oldroyd-B fluid, *J. Non-Newt. Fluid Mech.*, **94**(2-3), (2000), 179-203.

Sizaire, R., Lielens, G., Jaumain, I., Keunings, R. and Legat, V., On the Hysteretic Behavior of Dilute Polymer Solutions in Relaxation Following Extensional Flow, *J. Non-Newt. Fluid Mech.*, **82**(2-3), (1999), 233-254.

Smith, D.E. and Chu, S., The Response of Flexible Polymer Coils to a Sudden High Strain Rate Flow, *Science*, **281**, (1998), 1335-1340.

Smith, M.D., Armstrong, R.C., Brown, R.A. and Sureshkumar, R., Finite Element Analysis of Two-Dimensional Viscoelastic Flows to Three-Dimensional Perturbations, *J. Non-Newt. Fluid Mech.*, **93**(2-3), (2000), 203-244.

Solomon, M.J. and Muller, S.J., Flow past a sphere in polystyrene-based Boger fluids: The effect on the drag coefficient of finite extensibility, solvent quality and polymer molecular weight, *J. Non-Newt. Fluid Mech.*, **62**(1), (1996), 81-94.

Solomon, M.J. and Muller, S.J., The transient extensional behavior of polystyrene-based Boger fluids of varying solvent quality and molecular weight, *J. Rheol.*, **40**(5), (1996), 837-856.

Sridhar, T., Nguyen, D.A. and Fuller, G.G., Birefringence and Stress Growth in Uniaxial Extension of Polymer Solutions, *J. Non-Newt. Fluid Mech.*, **90**(2-3), (2000), 299-315.

Tehrani, M.A., An experimental study of particle migration in pipe flow of viscoelastic fluids, *J. Rheol.*, **40**(6), (1996), 1057-1077.

Tirtaatmadja, V., Uhlherr, P.H.T. and Sridhar, T., Creeping Motion of Spheres in Fluid M1, *J. Non-Newt. Fluid Mech.*, **35**, (1990), 327-337.

van den Brule, B.H.A.A., Brownian Dynamics Simulation of Finitely Extensible Bead-Spring Chains, *J. Non-Newt. Fluid Mech.*, (1993), 357-378.

van den Brule, B.H.A.A. and Gheissary, G., Effects of Fluid Elasticity on the Static and Dynamic Settling of a Spherical Particle, *J. Non-Newt. Fluid Mech.*, **49**(1), (1993), 123-132.

Walters, K. and Tanner, R.I., "The Motion of a Sphere Through an Elastic Liquid", Transport Processes in Bubbles, Drops and Particles, R. P. Chhabra and D. De Kee (ed.), Hemisphere Publ. Corp., New York, 1992.

Warichet, V. and Legat, V., Adaptive High-Order Prediction of the Drag Correction Factor for the Upper-Convected Maxwell Fluid, *J. Non-Newt. Fluid Mech.*, **73**, (1997), 95-114.

Watanabe, K., Kui, H. and Motosu, I., Drag of a sphere in dilute polymer solutions in high Reynolds number range, *Rheol. Acta*, **37**(4), (1998), 328-335.

White, S.A. and Baird, D.G., The Importance of Extensional Flow Properties on Planar Entry Flow Patterns of Polymer Melts, *J. Non-Newt. Fluid Mech.*, **20**, (1986), 93-101.

Yang, B. and Khomami, B., Simulations of sedimentation of a sphere in a viscoelastic fluid using molecular based constitutive models, *J. Non-Newt. Fluid Mech.*, **82**(2-3), (1999), 429-452.

Yuran, F. and Crochet, M.J., High-Order Finite-Element Methods For Steady Viscoelastic Flows, *J. Non-Newt. Fluid Mech.*, **57**(2-3), (1995), 283-311.

Zheng, R. and Phan-Thien, N., A Boundary Element Simulation of the Unsteady Motion of a Sphere in a Cylindrical Tube containing a Viscoelastic Fluid, *Rheol. Acta*, **31**, (1992), 323-332.

Zheng, R., Phan-Thien, N. and Tanner, R.I., The Flow Past a Sphere in a Cylindrical Tube: Effects of Inertia, Shear-thinning and Elasticity, *Rheol. Acta*, **30**, (1991), 499-510.

List of Figures

7. Interaction of elastic and inertial effects on the extent and strength of the negative wake behind a sphere sedimenting through a shear-thinning viscoelastic fluid (PAA/G/W). The elasticity number increases from $El \approx 460$ (❍) to $El \approx 0.77$ (□) (reproduced from Arigo & McKinley 1998).

8. The negative wake behind a sphere showing the sensitivity of the wake structure to the values of the rheological parameters. The instantaneous streamlines are shown in the stationary laboratory reference under equivalent conditions for a Newtonian fluid, the UCM fluid ($De = 1.5$), a FENE-CR model ($De = 1.5$; $L = 10$) (reproduced from Satrape & Crochet 1994)

9. Transient evolution in the sedimentation velocity $-U_s(t)$ of a sphere of density $\rho_s = 3.59$ g/cm^3 and $a = 1$ cm dropped from rest in tubes of different radius ratios (here denoted $\beta \equiv a/R$) containing an Oldroyd-B fluid with $\eta_s/\eta_0 = 1/2$ (———) and 1/9 (– – –) respectively (reproduced from Bodart & Crochet, 1994).

10. DPIV measurements of the transient evolution of the sedimentation velocity $U_s(t)$ and the viscoelastic wake for a sphere accelerating from rest in a 2.0 wt% PAA/G/W solution at $De = 2.3$; $Re = 0.005$ (based on the shear-rate-dependent viscometric properties). The radius ratio is $a/R = 0.243$; and $E_s \approx 189$. The sphere undergoes large amplitude but heavily damped oscillations at short times (a–f) before the formation of a negative wake at longer times (g-h). (reproduced from Arigo & McKinley 1998).

11. (a) Experimental observation of the interaction between two particles ($a = 3.175$ mm) initially separated by a distance $\delta = 3.84$ mm and sedimenting in a viscoelastic solution of 1.5 wt% PEO/G/W (reproduced from Joseph et al. 1994); (b) Stokesian dynamics calculations of particle-particle interaction in a dilute suspension of FENE dumbbells with $De \approx 3$, $L = 10$ (reproduced from Binous & Phillips, 1999).

12. Shear-induced alignment and aggregation in a 2% (vol.) suspension of glass spheres in a shear-thinning viscoelastic matrix fluid composed of 2% Polyox (PEO/W). The spheres are polydisperse with sizes $250 \le a \le 850$ μm and undergo shearing in a parallel plate device with gap $H = 2.1$ mm and a rim shear rate of $\dot{\gamma}_R = \Omega R/H \approx 19 s^{-1}$ (reproduced from Feng & Joseph, 1996).

13. Fluctuating velocity profile during sedimentation of a sphere through a 9 mM cetyltrimethyl-ammonium bromide/sodium salicylate (CTAB/NaSal) solution; (a) time-lapse sequence of

video images at constant spacing of $\delta t = 0.26$ s; (b) evolution in velocity profile of the sedimenting sphere (images provided by Jayaraman & Belmonte, 2001).

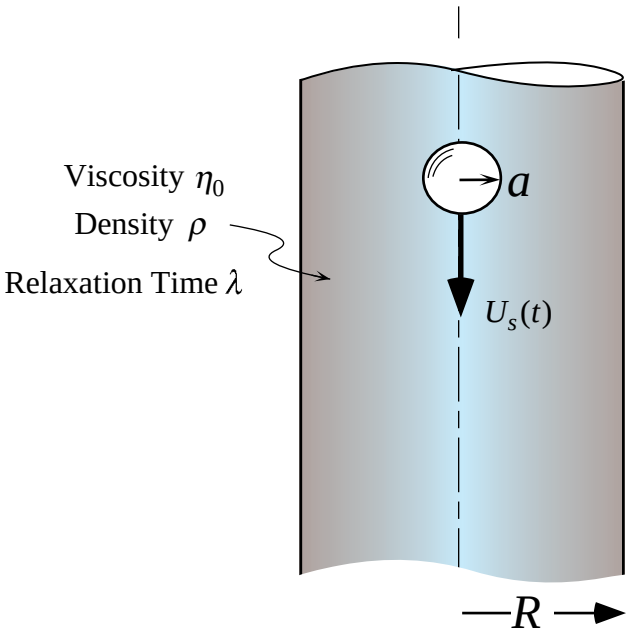

Figure 1
McKinley 2001

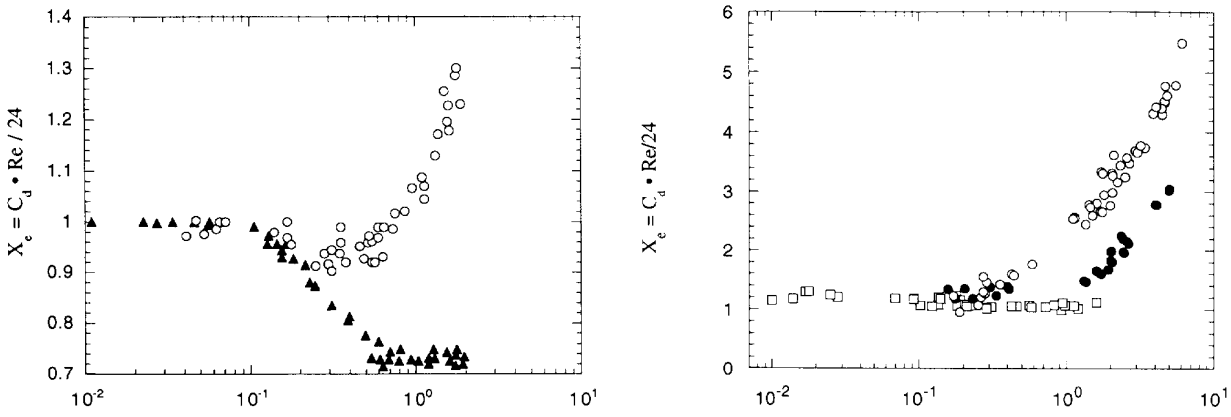

Figure 2
McKinley, 2001

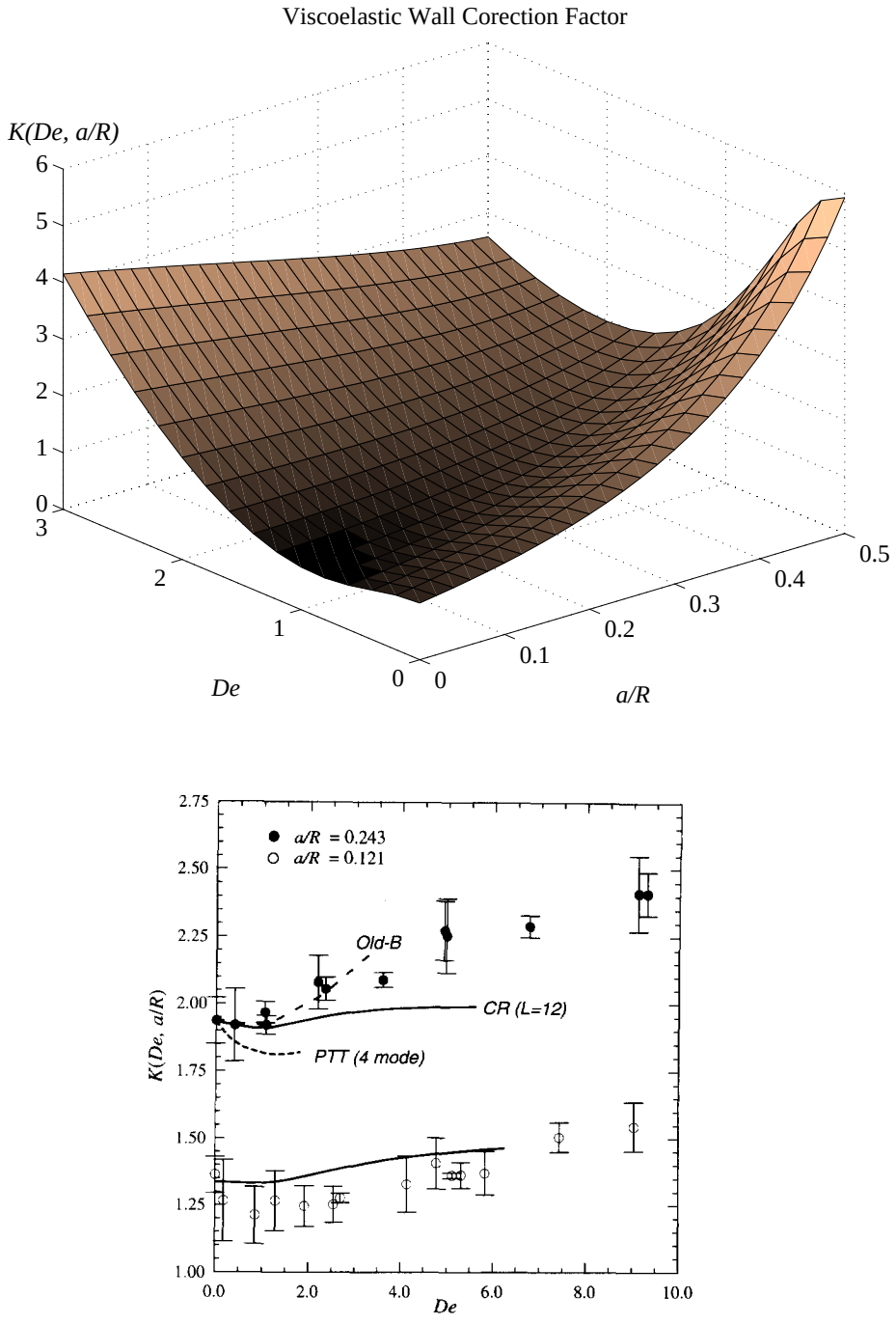

Figure 3
McKinley 2001

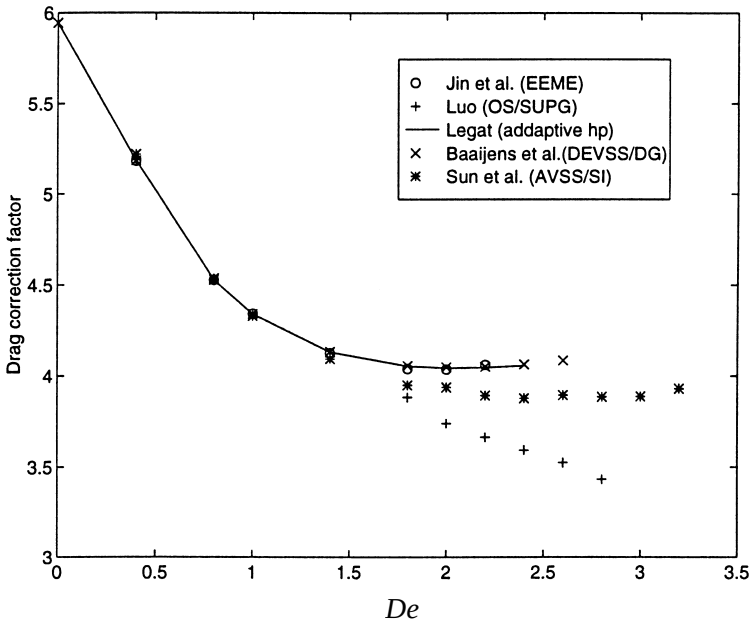

Figure 4
McKinley 2001

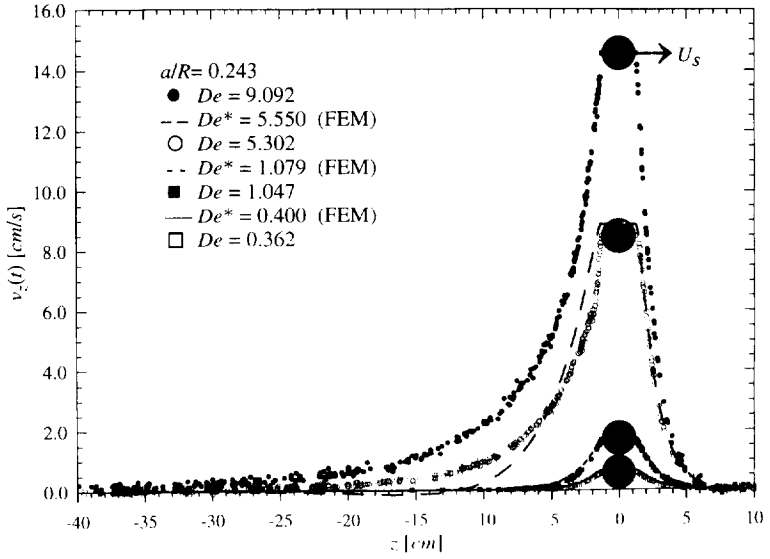

Figure 5
McKinley, 2001

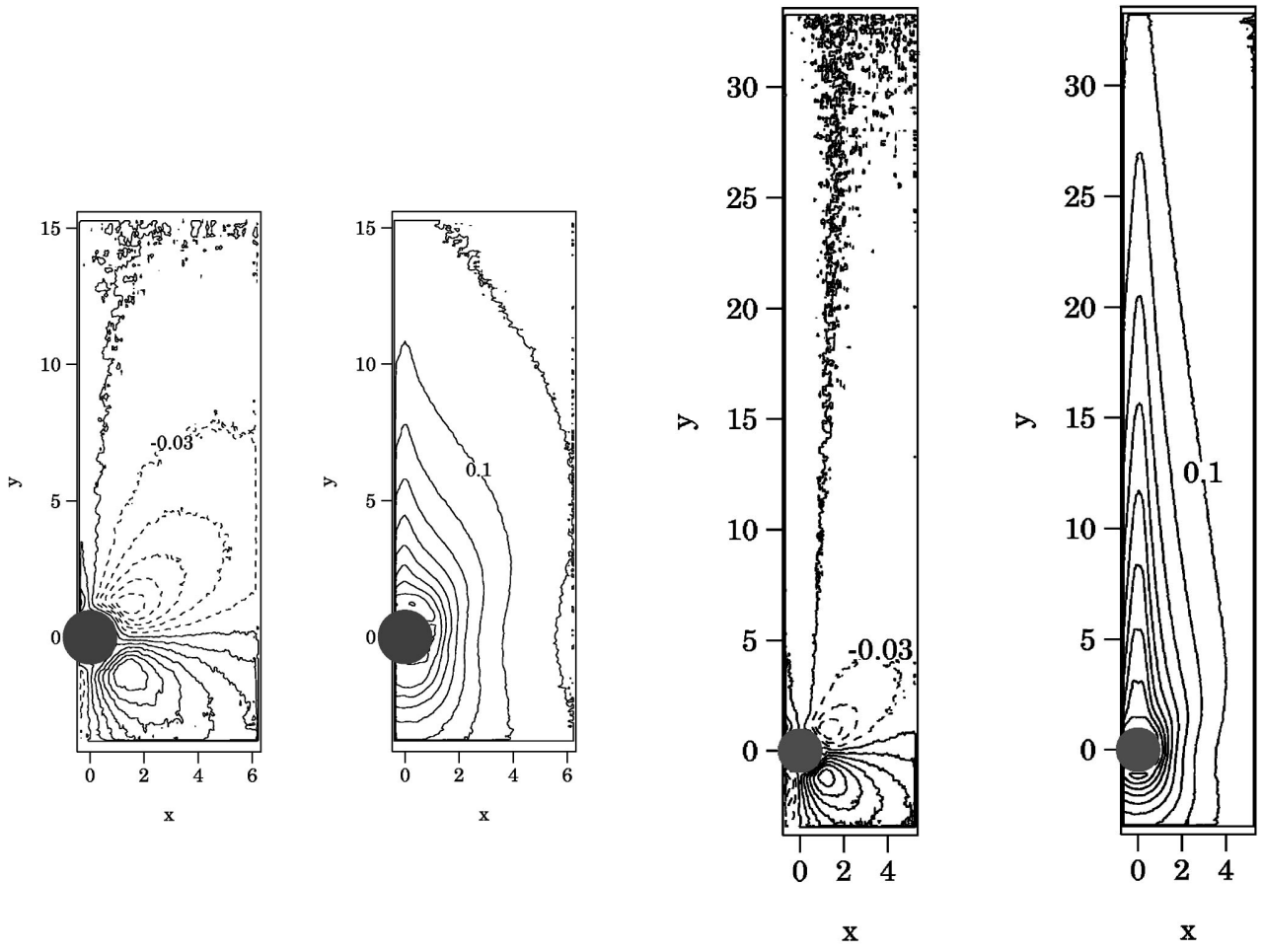

Figure 6
McKinley, 2001

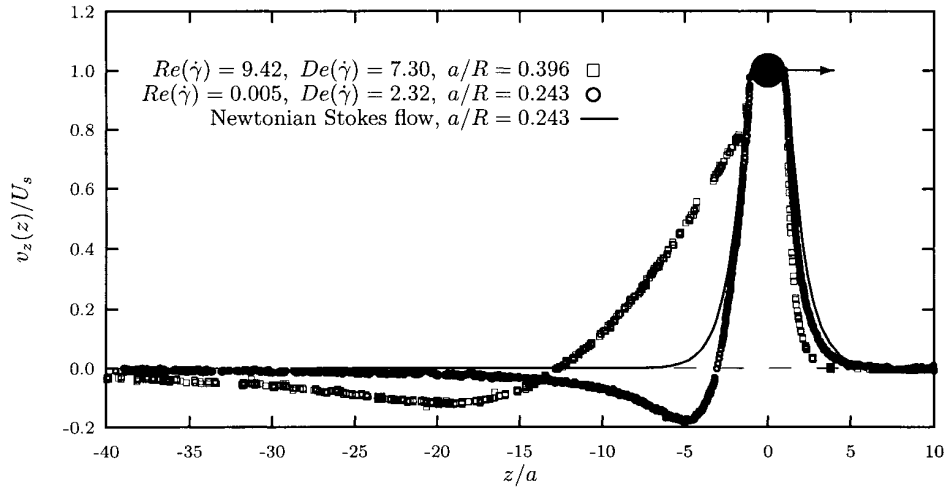

Figure 7
McKinley, 2001

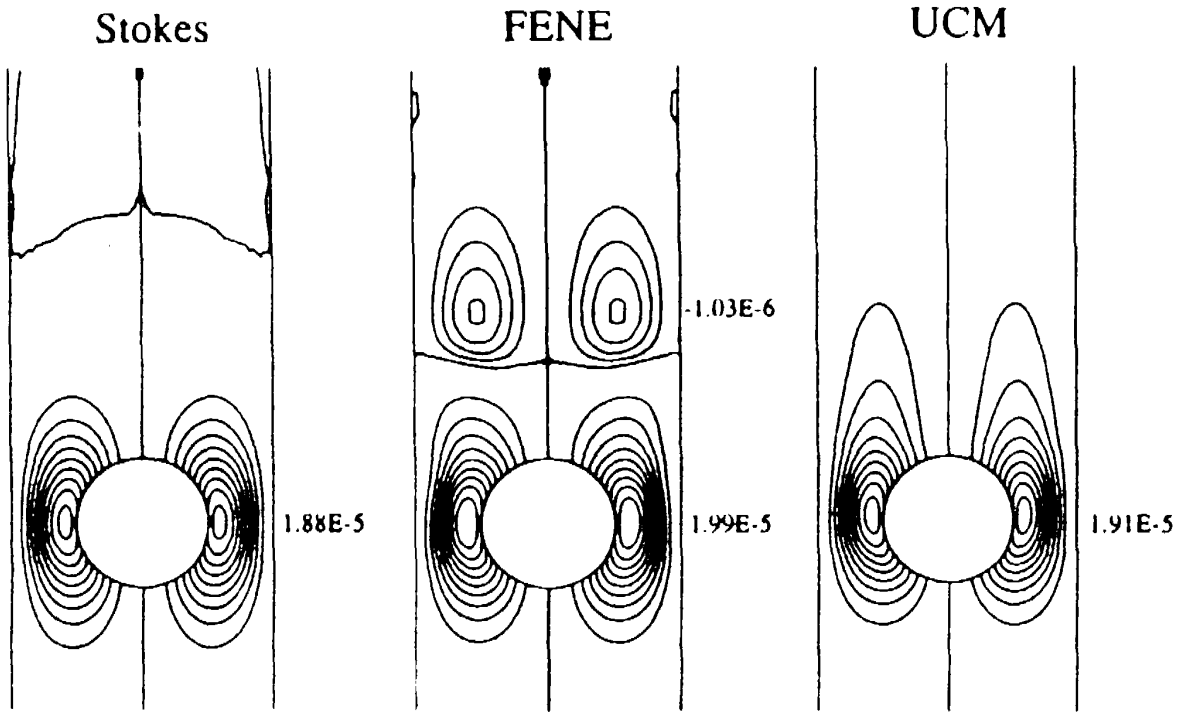

Figure 8
McKinley, 2001

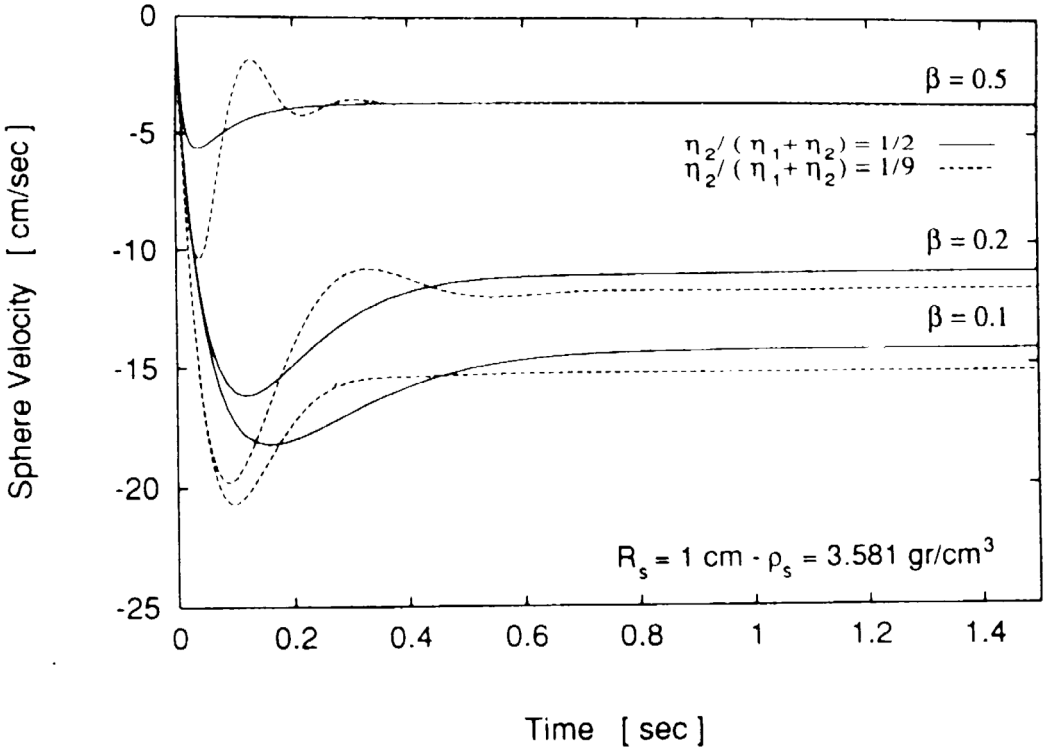

Figure 9
McKinley, 2001

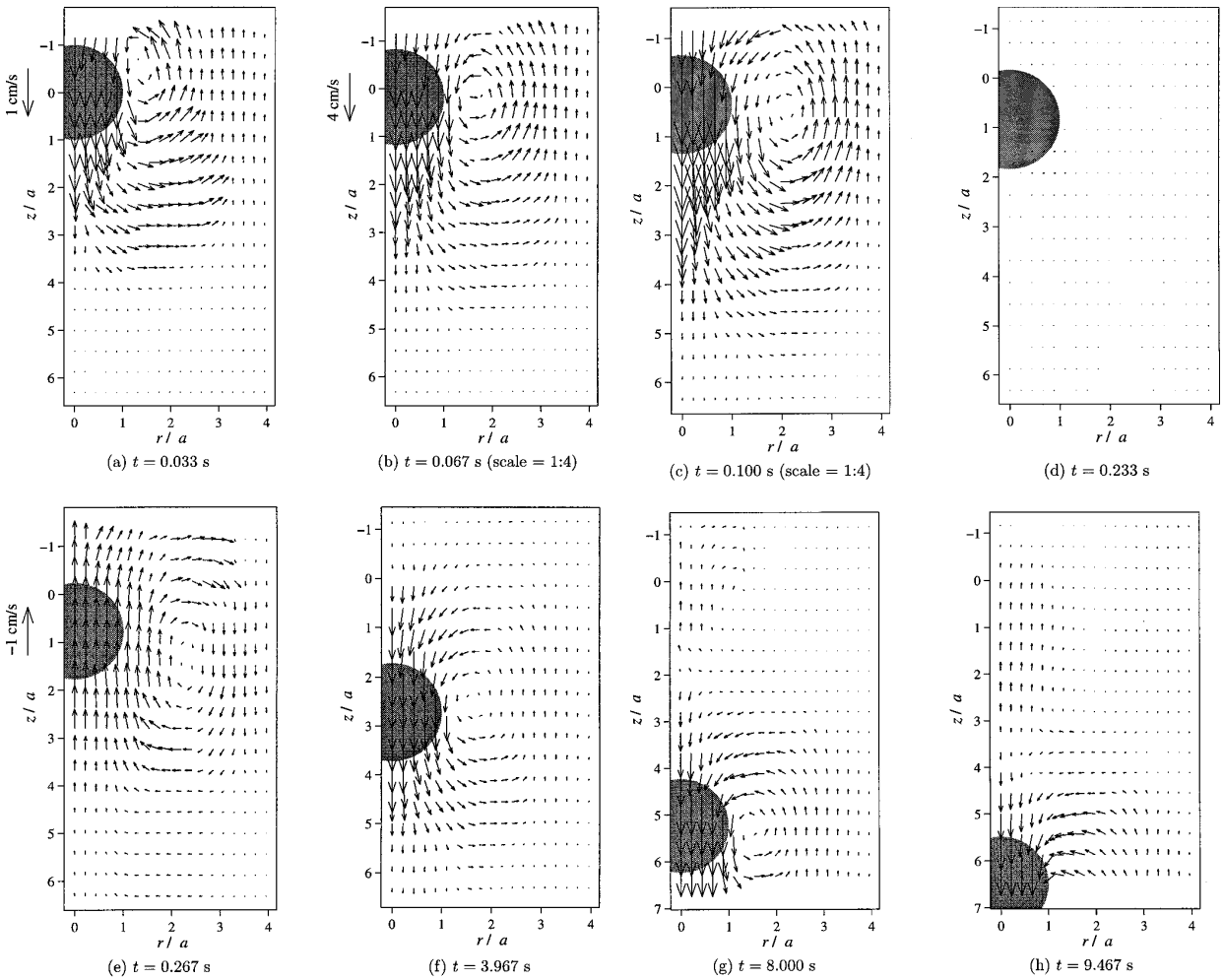

Figure 10
McKinley, 2001

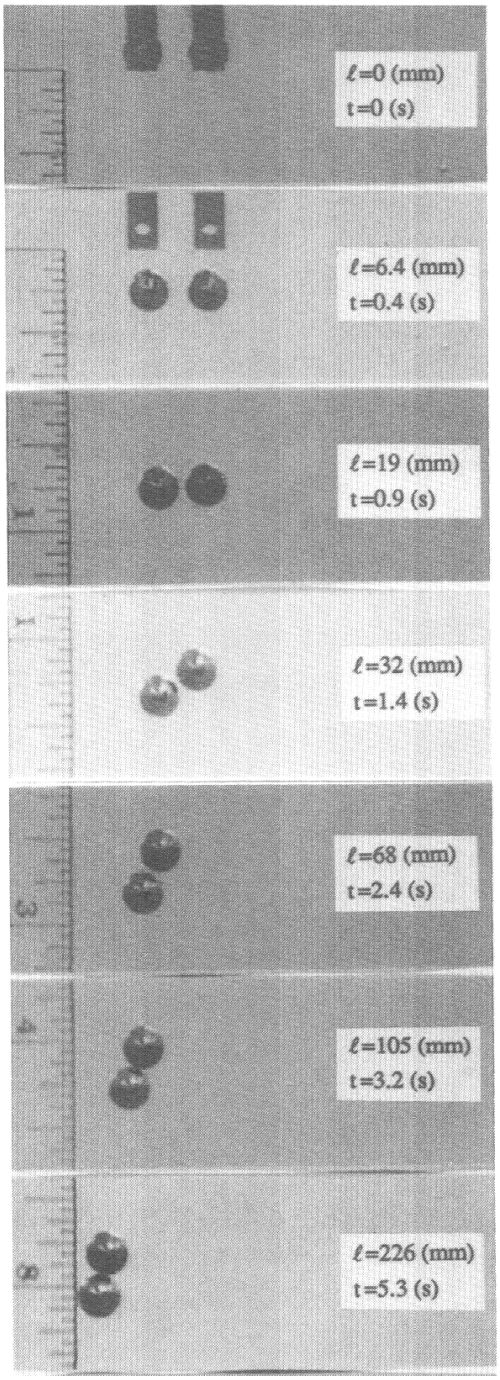

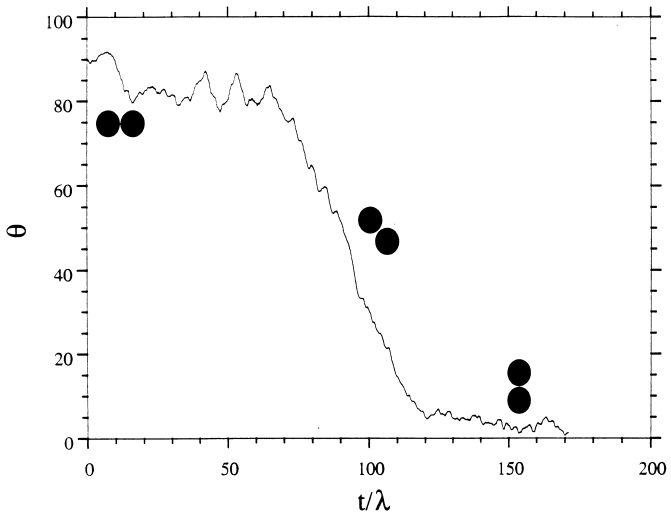

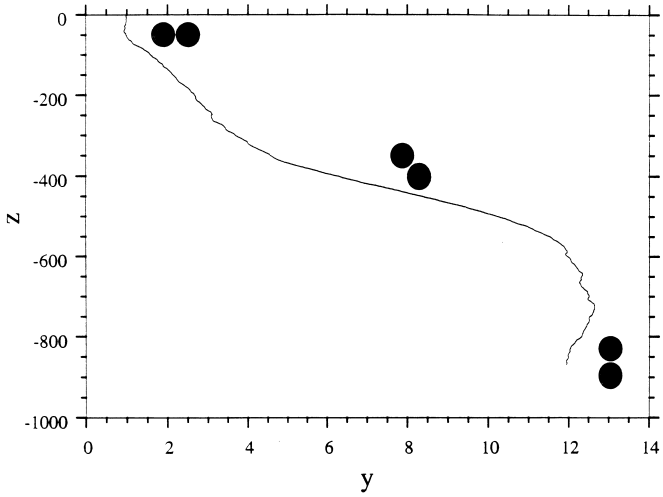

Figure 11
McKinley 2001

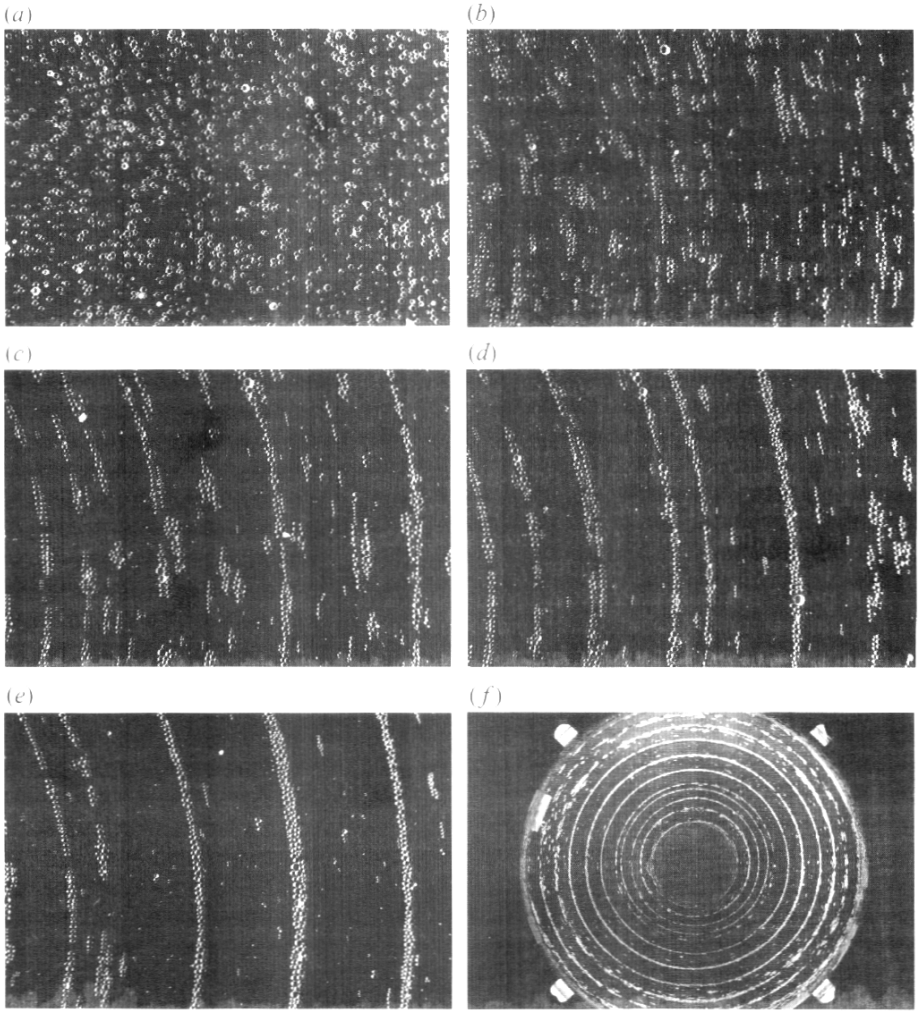

Figure 12
McKinley 2001

(a)

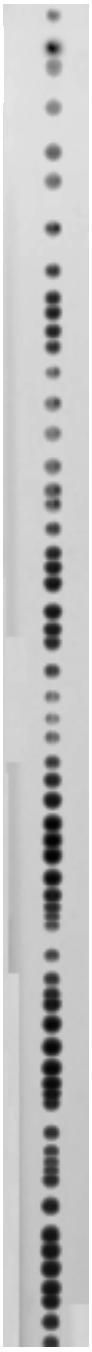

(b)

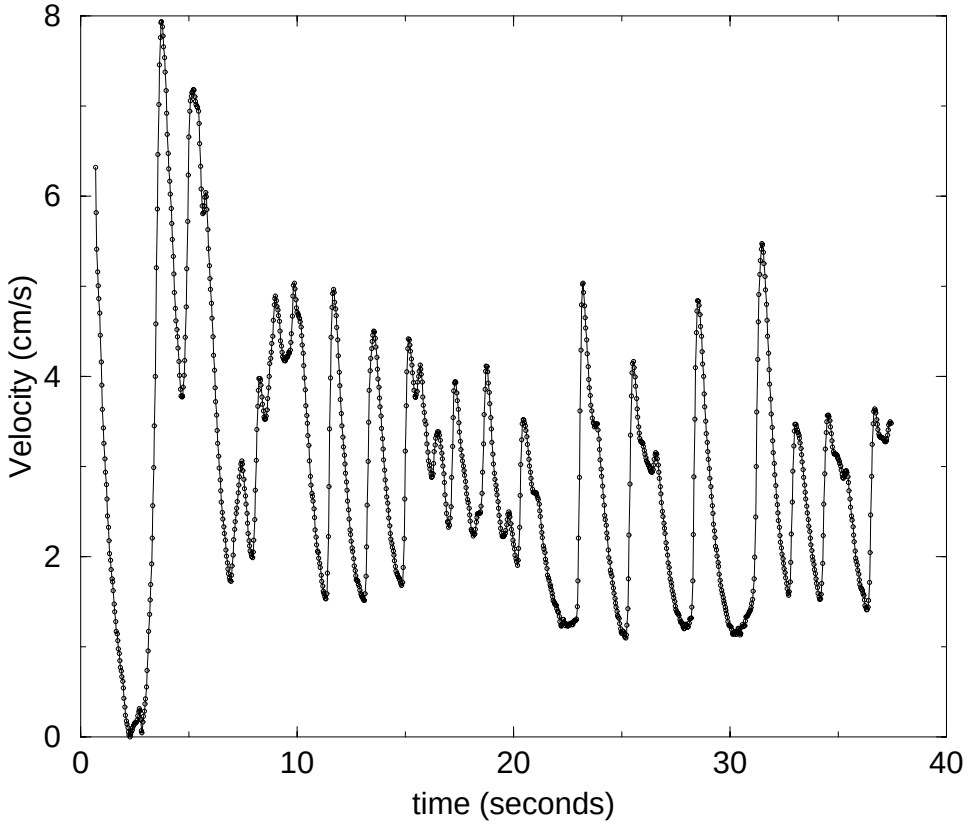

Figure 13
McKinley, 2001